1×10^6 cells/mL, incubated for 20 min with a fluorescein isothiocyanate (FITC)-conjugated antibody against CD49b or CD98 (BioLegend) or a phycoerythrin (PE)-conjugated antibody against CD10, CD13, CD29, CD44, CD49a, CD49c, CD49d, CD49e, CD51/61, CD73, CD90, CD105, CD117, SSEA4, HLA-A,B,C (BioLegend), CD133/1 (Miltenyi Biotec), or CD166 (Beckman Coulter). Nonspecific staining was assessed using relevant isotype controls. Dead cells were excluded using the Live/Dead Fixable Far Red Dead Cell Stain Kit (Life Technologies). FlowJo software was used for quantitative analysis.

RNA extraction, cDNA generation, and quantitative polymerase chain reaction

Total RNA was extracted using the RNeasy Mini Kit (Qiagen) accroding to the manufacturer's instructions. cDNA was generated from 1 μg of total RNA using the Verso cDNA Synthesis Kit (Thermo Scientific) and purified using the MinElute PCR Purification Kit (Qiagen). Quantitative polymerase chain reaction (Q-PCR) analysis was conducted using the SsoFast EvaGreen supermix (Bio-Rad) according to the manufacturer's protocols. The relative expression value for each gene was calculated using the ΔΔCt method, and the most reliable internal control gene was determined using geNorm Software (http://medgen.ugent.be/~jvdesomp/genorm/). Details of the primers used in these experiments are available on request.

Western blot analysis

Whole cell extracts were prepared by washing cells with ice-cold PBS and lysing them with M-PER Mammalian Protein Extraction Reagent (Thermo Scientific Pierce) according to the manufacturer's instructions. Nuclear and cytosolic extracts were prepared as follows. Cells were washed with ice-cold PBS and lysed with lysis buffer (50 mM Tris-HCl (pH 7.5), 0.5% Triton X-100, 137.5 mM NaCl, 10% glycerol, 5 mM EDTA, 1 mM sodium vanadate, 50 mM sodium fluoride, 10 mM sodium pyrophosphate, and protease inhibitor cocktail). Then, insoluble nuclei were isolated by centrifugation and lysed with lysis buffer containing 0.5% SDS. Equal amounts of proteins were separated by sodium dodecyl sulfate polyacrylamide gel electrophoresis (SDS-PAGE), transferred to polyvinylidene fluoride membranes (Immobilon-P; Millipore), and probed with antibodies against cleaved Notch1 (#2421; Cell Signaling Technology), HIF-1α (#610959; BD Bioscience), hypoxia-inducible factor 2α (MAB3472; Millipore), Akt (#9272; Cell Signaling Technology), and phospho Akt (Ser473) (#4060; Cell Signaling Technology). Horseradish peroxidase (HRP)-conjugated anti-mouse or -rabbit IgG antibody (Cell Signaling Technology) was used as a secondary antibody, and immunoreactive bands were visualized using Immobilon Western Chemiluminescent HRP substrate (Millipore). The band intensity was measured using the ImageJ software.

Fluorescence microscopy

Phase-contrast and fluorescence images were obtained using a fluorescence microscope (BZ-9000; Keyence) using BZ Analyzer Software (Keyence).

Adipogenic, osteogenic, and chondrogenic differentiation procedures

For adipogenic differentiation, cells were cultured in differentiation medium (Zen-Bio). After 7 days, half of the medium was exchanged for adipocyte medium (Zen-Bio) and this was repeated every 3 days. Three weeks after differentiation, adipogenic differentiation was confirmed by a microscopic observation of intracellular lipid droplets with the aid of Oil Red O staining. Osteogenic differentiation was induced by culturing the cells in osteocyte differentiation medium (Zen-Bio). Differentiation was examined by Alizarin Red staining. For chondrogenic differentiation, 2×10^5 hADMSCs were centrifuged at 400 *g* for 10 min. The resulting pellets were cultured in chondrogenic medium (Lonza) for 21 days. The pellets were fixed with 4% paraformaldehyde in PBS, embedded in OCT, frozen, and sectioned at 8 μm. The sections were incubated with PBSMT (PBS containing 0.1% Triton X-100, and 2% skim milk) for 1 h at room temperature, and then incubated with a mouse monoclonal antibody against type II collagen (Abcam) for 1 h. After washing with PBS, cells were incubated with Alexa 546-conjugated anti-mouse IgG to identify chondrocytes (Life Technologies). The cells were counterstained with 4′-6-diamidino-2-phenylindole (DAPI) (Life Technologies) to identify cellular nuclei. The sections were also stained with 1% alcian blue (Sigma Aldrich) in 3% acetic acid, pH 2.5 for 30 min.

Determination of HK, PFK, LDH, PDH, and Cox IV activities

Cells (2×10^6) were lysed, and HK, PFK, LDH, or PDH activity was measured using the Hexokinase Colorimetric Activity Kit, Phosphofructokinase (PFK) Activity Colorimetric Assay Kit, Lactate Dehydrogenase (LDH) Activity Assay Kit, or Pyruvate Dehydrogenase Activity Colorimetric Assay Kit (all from BioVision), respectively, according to the manufacturer's instructions. To measure Cox IV activity, mitochondria were isolated from 2×10^7 cells using a Mitochondria Isolation Kit (Thermo Scientific) and lysed with buffer containing n-Dodecyl β-D-maltoside, followed by measurement with the Mitochondria Activity Assay (Cytochrome C Oxidase Activity Assay) Kit (BioChain Institute), according to the manufacturer's instructions.

Results

5% oxygen hypoxic culture condition increases proliferation capacity and decreases senescence

hADMPCs were cultured under 20% oxygen (normoxia; Nx) or 5% oxygen (hypoxia; Hx), and their proliferation capacities were examined based on the relationship between the number of cultivation days and the population doubling level (PDL). Nx-cultured hADMPCs ceased proliferation at a PDL of 35–40 (between 46–70 days), whereas continuous cell proliferation beyond 45 PDL was observed when hADMPCs were cultured in the Hx condition (Fig. 1A). To investigate whether this increase of PDL in the Hx culture condition resulted from an increase in cell cycle progression and increase in survival rates, EdU, an alternative to 5-bromo-2′-deoxyuridine (BrdU), was incorporated into the

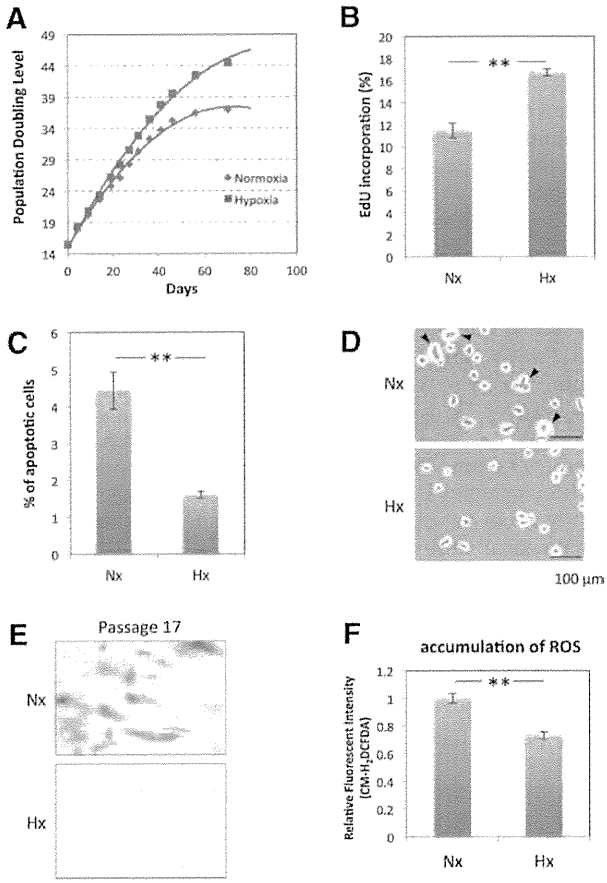

FIG. 1. Hypoxia increases proliferation capacity and decreases senescence in tissue-derived multilineage progenitor cells (hADMPCs). **(A)** Growth profiles of hADMPCs under normoxic (*red square*) and hypoxic (*blue square*) conditions. The population doubling level (PDL) was determined to be 0 when cells were isolated from human adipose tissue. Cells were maintained until they reached PDL13–15 (passage 3) and then split into four aliquots of equal cell densities. PDL was calculated based on the total cell number at each passage. **(B)** Detection of normoxic (Nx) and hypoxic (Hx) cells by flow cytometry after incorporation of EdU. **(C)** Percentages of apoptotic cells with sub-G1 DNA under Nx and Hx conditions. The results are presented as the mean of three independent experiments. **(D)** hADMPCs cultured under Nx and Hx conditions were harvested by trypsin-EDTA and then imaged using a phase-contrast microscope. *Arrowheads* indicate cells with a larger and more irregular shape. **(E)** Cells expanded under Nx and Hx conditions were stained with SA-β-gal. **(F)** Cellular reactive oxygen species detection by the oxidative stress indicator CM-H_2DCFDA in hADMPCs under Nx or Hx. Data are presented as the mean fluorescence intensity of three independent experiments. Error bars indicate SD. $^{**}P<0.01$ indicates significant difference (independent *t*-test) between Nx and Hx. Scale bars; 100 μm. Color images available online at www.liebertpub.com/scd

genomic DNA of the hADMPCs, and the amount of incorporated EdU was quantified by flow cytometry. As shown in Fig.1B, the EdU incorporation rate was significantly higher in Hx-cultured hADMPCs than in Nx-cultured hADMPCs, suggesting that cell growth was increased in the Hx culture condition. In addition, measurement of DNA content in hADMPCs revealed a slight but significant decrease of sub-G1 peaks, which indicates the existence of apoptotic cells with degraded DNA, when the cells were cultured in the Hx condition (Fig. 1C). These data suggest that the Hx culture condition increases the proliferation capacity of hADMPCs by promoting their cell growth and survival rates. We also found that Nx-cultured hADMPCs were larger with a more irregular shape (Fig. 1D), which suggests that the Hx culture condition prevented hADMPCs from entering senescence [35]. To further investigate this phenomenon, cellular senescence was measured by staining for SA-β-Gal, which revealed that SA-β-Gal activity was increased in Nx-cultured hADMPCs at passage 17 (Fig. 1E). Since it has been hypothesized that senescence results from oxidative stress [20], accumulation of ROS in hADMPCs was detected using the nonfluorescent probe, CM-H_2DCFDA. Flow cytometry analysis revealed that ROS were generated at higher levels in hADMPCs when cultured in the Nx condition (Fig. 1F), suggesting that reduced production of ROS in the Hx condition may prevent the cells from entering replicative senescence.

Hypoxic culture maintains some MSC properties and increases differentiation

We then examined the cell properties of hADMPCs under Nx and Hx conditions. Initially, cell surface antigens expressed on hADMPCs were analyzed by flow cytometry. No significant difference in expression profile between hADMPCs cultured in Nx and Hx was observed; the cells were consistently positive for CD10, CD13, CD29, CD44, CD49a, CD49b, CD49c, CD49d, CD49e, CD51/61, CD54, CD59, CD73, CD90, CD98, CD105, CD166, and HLA-A, B, C, but negative for CD34, CD45, CD117, and CD133 (Fig. 2 and data not shown). These data were consistent with previous reports describing the expression profiles of cell surface markers of hMSCs [36,37]. To further examine the stem cell properties of hADMPCs, their potential for differentiation into adipocyte, osteocyte, and chondrocyte lineages was analyzed at passage 8. Hx-cultured hADMPCs presented enhanced differentiation into various lineages (Fig. 3A, B), indicating that the Hx culture condition improved the stem cell properties of hADMPCs.

Hypoxic culture condition activates Notch signaling

To reveal the molecular mechanism by which the Hx culture condition increased the proliferative capacity and maintained the stem cell properties of hADMPCs, we next examined Notch signaling, which is required for maintaining stem-cell features of various types of stem cells [30,31]. As expected, levels of cleaved NOTCH1, an activated form of NOTCH1, were significantly increased (greater than twofold) in the Hx culture condition (Fig. 4A). Q-PCR analysis revealed that HES1, a downstream target of Notch signaling, was upregulated in Hx-cultured hADMPCs, which also indicated that Notch signaling was activated in

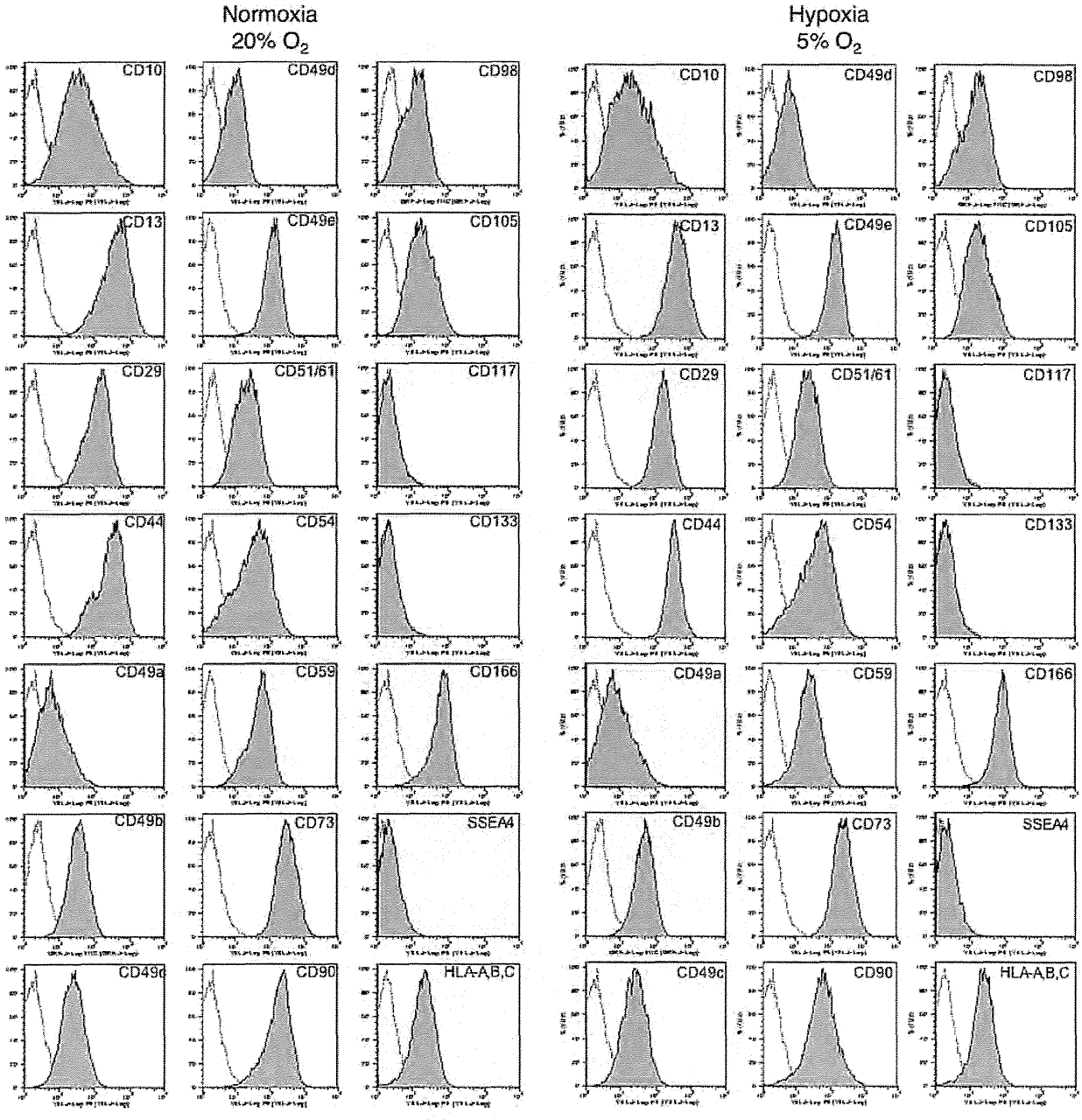

FIG. 2. Hypoxic culture maintains mesenchymal stem cell properties. hADMPCs cultured under normoxia (20% O_2) or hypoxia (5% O_2) were labeled with antibodies against the indicated antigens and analyzed by flow cytometry. Representative histograms are shown. The respective isotype control is shown as a *gray line*.

the Hx culture condition (Fig. 4B). Administration of the γ-secretase inhibitor DAPT at 1 μM, which was sufficient to inhibit the proteolytic cleavage of NOTCH1 (Fig. 4A), decreased the Hx-induced expression of HES1 at both mRNA and protein levels (Fig. 4B, C). These data indicate that Hx increased the expression of HES1 through activation of Notch signaling. It has been reported that Notch signaling and hypoxia-inducible factor (HIF) undergo crosstalk in hypoxic cells [38–41]. Therefore, HIF-1α and HIF-2α protein levels in hADMPCs were analyzed by western blotting. HIF-1α was stabilized when a chemical hypoxia-mimicking agent, cobalt chloride, was applied in the culture; whereas no obvious increase of HIF-1α was observed in the Hx culture condition (Fig. 4D). However, we did not detect any HIF-2α expression even in the presence of cobalt chloride (Fig. 4E). Q-PCR analysis revealed that *HIF2A* mRNA was not expressed in these cells (data not shown). From these results, we concluded that neither HIF-1α nor HIF-2α was involved in the Hx-induced increase in the proliferative capacity and stem cell properties of hADMPCs.

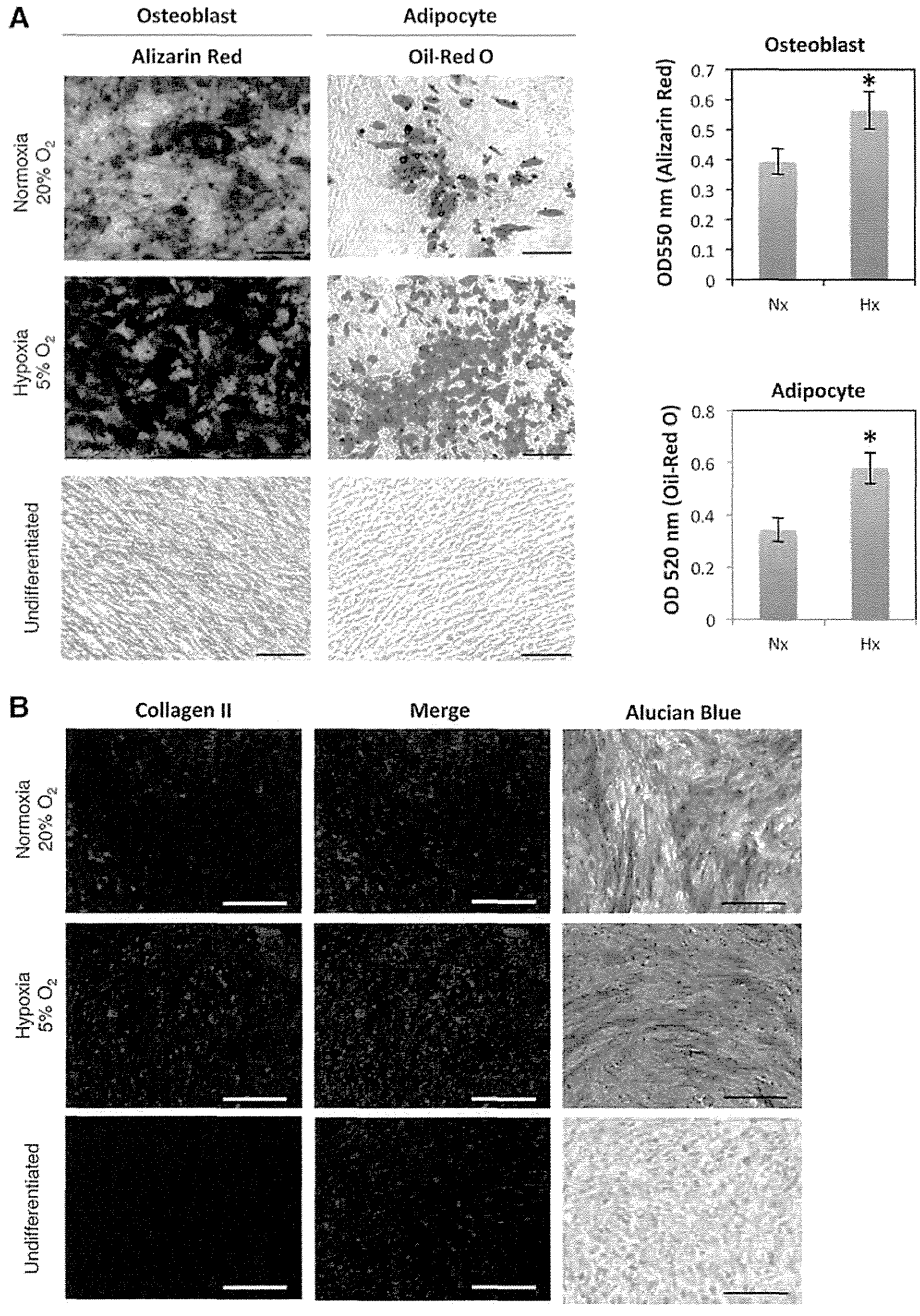

FIG. 3. Hypoxic culture enhances stem cell properties. hADMPCs were expanded under normoxic and hypoxic conditions. **(A)** Normoxic (20% O_2) and hypoxic (5% O_2) cells at passage 8 were induced for 3 weeks to differentiate into osteoblasts and adipocytes and stained with Alizarin Red and Oil-Red O, respectively. The stained dye was extracted, and OD values were measured and plotted as the means of three independent experiments ± SD. $^*P < 0.05$. Scale bars, 200 μm. **(B)** Normoxic (20% O_2) and hypoxic (5% O_2) cells at passage 8 were induced for 3 weeks to differentiate to chondrocytes, and immunofluorescent analysis of collagen II (*red*) and Alucian Blue staining were performed. The *blue* signals indicate nuclear staining. Scale bars, 100 μm. Non-induced control cultures in growth medium without adipogenic, osteogenic or chondrogenic differentiation stimuli are shown (Undifferentiated). Color images available online at www.liebertpub.com/scd

To identify the signaling responsible for the observed effect, we next examined the Akt, NF-κB, and p53 signaling pathways. It has been reported that hypoxic conditions induce the activation of Akt and NF-κB signaling [42,43]. In addition, hypoxic conditions have been shown to inhibit p53 activity [44], and crosstalk between these pathways and Notch signaling has also been demonstrated [41,45–47]. As shown in Fig. 4F, the Hx condition increased Akt phosphorylation, which was not decreased by DAPT treatment. These data demonstrate that 5% oxygen activated Akt signaling but not via Notch signaling. Similarly, the hypoxic condition induced nuclear accumulation of p65, which was inhibited by DAPT treatment (Fig. 4G). These data suggest that NF-κB signaling is regulated by Notch signaling in hADMPCs. Furthermore, p53 was not activated under the 5% oxygen condition as assessed by detection of phospho-p53 and a p53 reporter assay. However, DAPT treatment significantly increased p53 activity (Fig. 4H, I).

Notch signaling is indispensable for acquisition of the advantageous properties of hADMPCs

We next examined the roles of Notch signaling in the proliferative capacity and stem cell properties of hADMPCs

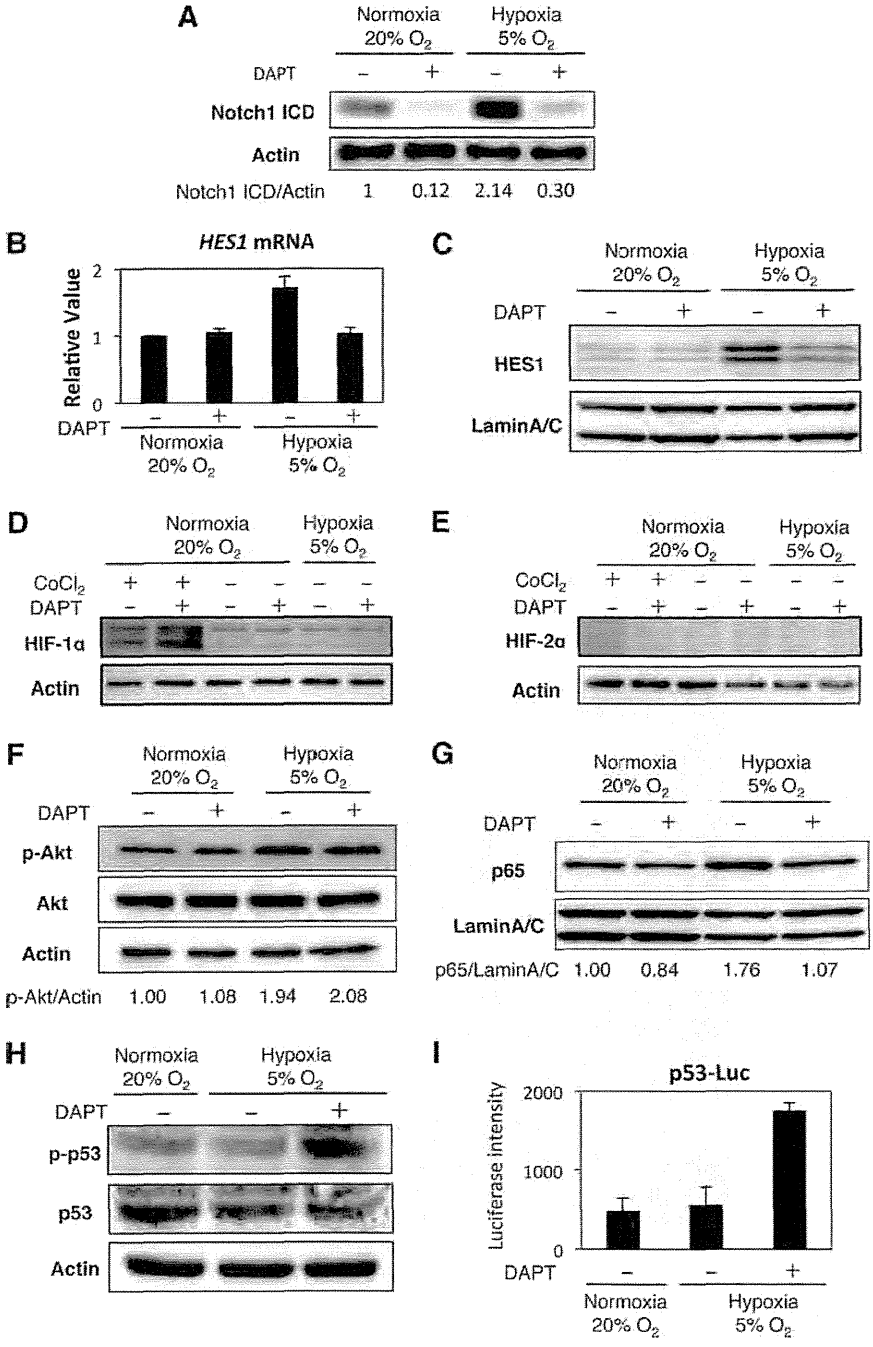

FIG. 4. Hypoxic culture condition activates Notch signaling but not HIF proteins. hADMPCs were expanded under normoxic (20% O_2) and hypoxic (5% O_2) conditions. DAPT (1 μM) was added to inhibit Notch signaling. **(A)** Western blot analysis of intracellular domain of Notch1 (Notch1 ICD) expression. Actin served as the loading control. Numbers below blots indicate relative band intensities as determined by ImageJ software. **(B)** Q-PCR analysis of *HES1*. Each expression value was calculated with the ΔΔCt method using *UBE2D2* as an internal control. **(C)** Western blot analysis of HES1 in nuclear fractions of hADMPCs. Lamin A/C served as the loading control. **(D, E)** Western blot analysis of HIF-1α **(D)** and HIF-2α **(E)**. Cobalt chloride ($CoCl_2$) was added at a concentration of 100 μM to stabilize HIF proteins (positive control). **(F)** Western blot analysis of phosphorylated Akt (p-Akt) and Akt. Actin served as the loading control. Numbers below blots indicate relative band intensities as determined by ImageJ software. **(G)** Western blot analysis of nuclear localization of p65. Lamin A/C served as the loading control. Numbers below blots indicate relative band intensities as determined by ImageJ software. **(H)** Western blot analysis of phosphorylated p53 (p-p53) and p53. Actin served as the loading control. **(I)** Activity of p53 was measured by the p53-luciferase reporter assay. Relative luciferase activity was determined from three independent experiments and normalized to pGL4.74 activity.

in the Hx culture condition. To inhibit Notch signaling, DAPT was added to the medium at a final concentration of 1 μM. DAPT treatment significantly decreased the PDL when hADMPCs were cultured under either 20% or 5% oxygen (Fig. 5A). Intriguingly, measurement of the DNA content in hADMPCs revealed that inhibition of Notch signaling by 1 μM DAPT significantly attenuated the decrease in apoptotic cells in the Hx condition (Fig. 5B). These data suggest that 5% oxygen increases the proliferation capacity of hADMPCs through Notch signaling by promoting their survival. To examine whether Notch signaling affects the stem cell properties of hADMPCs, differentiation into adipocyte, osteocyte, and chondrocyte lineages was analyzed at passage 8. Hx-cultured hADMPCs underwent greater differentiation into all lineages as described in Fig. 3, whereas application of a Notch inhibitor significantly decreased the differentiation capacity to all lineages (Fig. 5C–E). In addition, SA-β-Gal staining revealed that inhibition of Notch signaling by DAPT remarkably promoted senescence in both the Nx and Hx

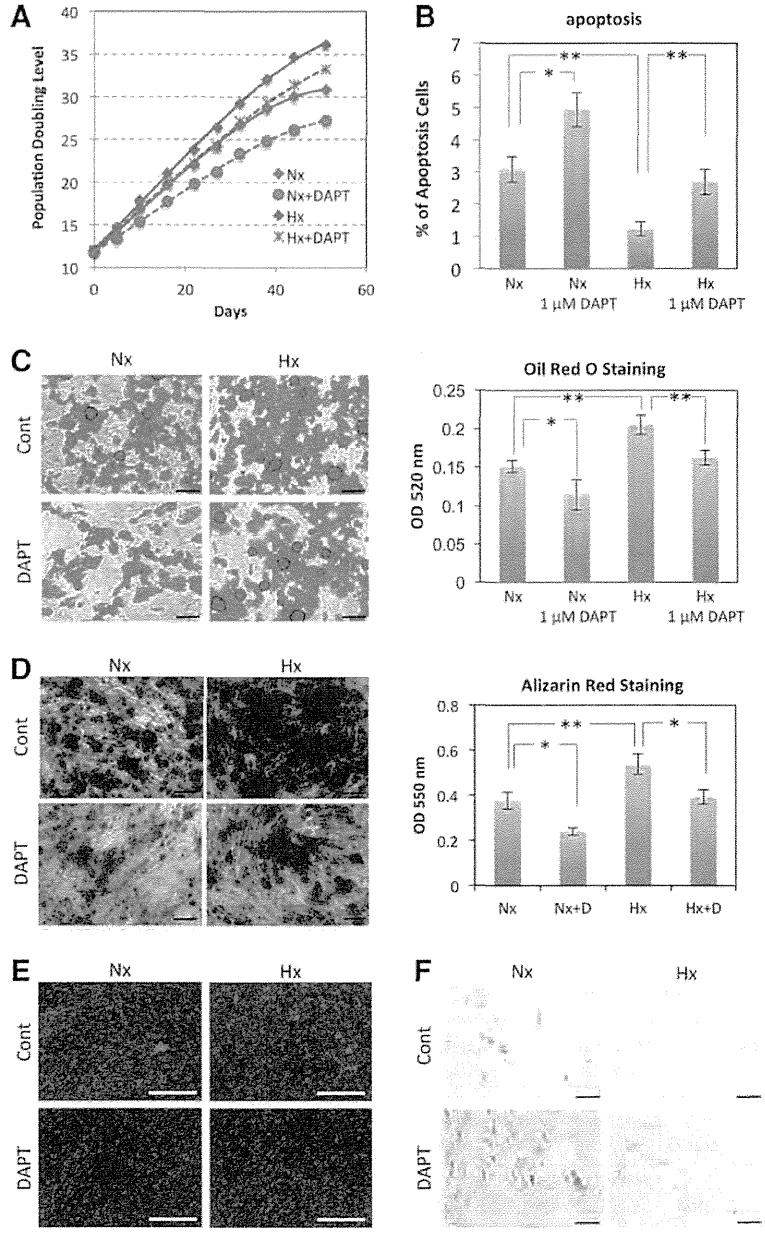

FIG. 5. Notch signaling is indispensable for acquisition of the advantageous properties of hADMPCs. hADMPCs were expanded under normoxic (20% O_2; Nx) and hypoxic (5% O_2; Hx) conditions. DAPT (1 μM) was added to inhibit Notch signaling. **(A)** Growth profiles of hADMPCs under Nx (*red*) and Hx (*blue*) conditions. *Solid lines* represent control cells, and *dotted lines* represent DAPT-treated cells. The number of population doublings was calculated based on the total cell number at each passage. **(B)** Percentages of apoptotic cells with sub-G1 DNA. Results are presented as the mean of three independent experiments ± SD. **(C, D)** hADMPCs at passage 8 were induced for 3 weeks to differentiate into adipocytes **(C)** and osteoblasts **(D)** and stained with Oil Red O and Alizarin Red, respectively. The stained dye was extracted, and OD values were measured and plotted as the means of three independent experiments ± SD. **(E)** hADMPCs at passage 8 were induced for 3 weeks to differentiate into chondrocytes, and an immunofluorescent analysis of collagen II (*red*) was performed. The *blue* signals indicate nuclear staining. **(F)** hADMPCs were stained with SA-β-gal. $*P < 0.05$ and $**P < 0.01$ indicate significant differences (independent *t*-test) between Nx and Hx. Scale bars; 100 μm. Color images available online at www.liebertpub.com/scd

culture conditions, suggesting that the suppression of replicative senescence observed in the Hx condition is mediated by Notch signaling (Fig. 5F).

Glycolysis is enhanced in the 5% oxygen condition through Notch signaling

Recent studies suggest that the metabolic shift from aerobic mitochondrial respiration to glycolysis extends the life span possibly via reduction of intrinsic ROS production [18,19]. Our results demonstrate that the 5% oxygen condition reduced ROS accumulation in hADMPCs (Fig. 1F). In addition, the relationship between Notch signaling and glycolysis has been recently established [48,49]. We, therefore, considered glycolytic flux by measuring the glucose consumption and lactate production of hADMPCs in the Nx or Hx culture conditions. As shown in Fig. 6A, glucose consumption and lactate production were elevated in the Hx culture condition, indicating that a metabolic shift to glycolysis occurred when hADMPCs were cultured in 5% oxygen. In contrast, the Notch inhibitor DAPT markedly reduced glycolytic flux as assessed by glucose consumption and lactate production (Fig. 6A). To identify the genes responsible for the glycolytic change, we performed a Q-PCR analysis. As shown in Fig. 6B, *SLC2A3, TPI, and PGK1*, encoding glycolytic enzymes, were upregulated in the 5% oxygen condition; whereas these genes were suppressed by DAPT treatment. Interestingly, Hes1 transduction by an adenoviral vector markedly induced the mRNA expression of the same genes (Fig. 6E). In addition, SCO2, a positive

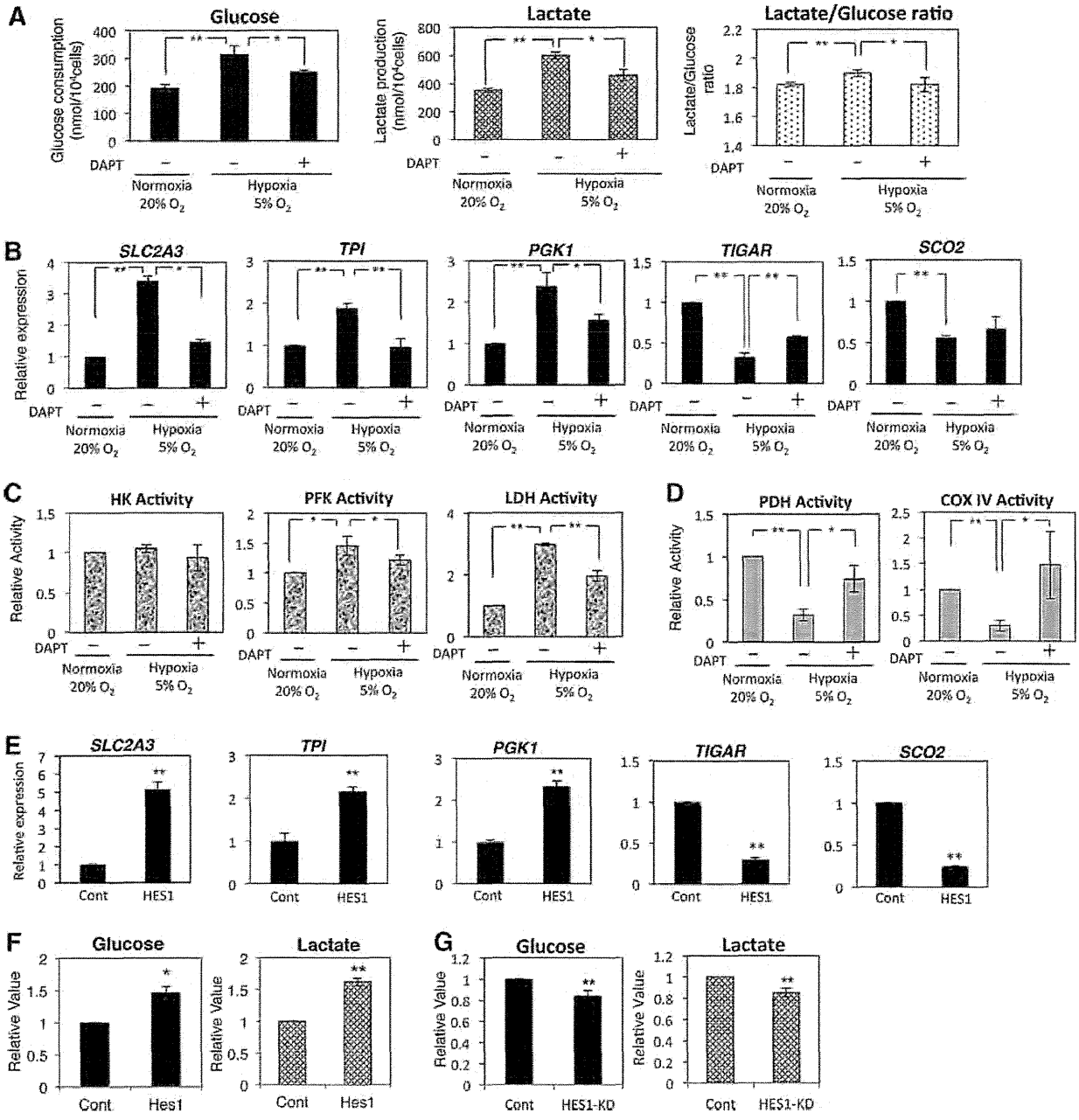

FIG. 6. Glycolysis is enhanced under 5% oxygen through Notch signaling. **(A–D)** hADMPCs were expanded under normoxic (20% O_2) and hypoxic (5% O_2) conditions. DAPT (1 μM) was added to inhibit Notch signaling. **(A)** Glucose consumption and lactate production of hADMPCs were measured and plotted as the means of three independent experiments ± SD. **(B)** Relative mRNA expression of *SLC2A3*, *TPI*, *PGK1*, *TIGAR*, and *SCO2* in hADMPCs. Each expression value was calculated with the ΔΔCt method using *UBE2D2* as an internal control. **(C, D)** Hexokinase (HK), phosphofructokinase (PFK), lactate dehydrogenase (LDH) **(C)**, pyruvate dehydrogenase (PDH), and Complex IV (Cox IV) **(D)** activities were measured and the value of relative activity was plotted as the means of three independent experiments ± SD. **(E, F)** hADMPCs were transduced with either mock (Cont) or HES1 and then cultured for 3 days. **(E)** Relative mRNA expression of *SLC2A3*, *TPI*, *PGK1*, *TIGAR*, and *SCO2* in hADMPCs. Each expression value was calculated with the ΔΔCt method using *UBE2D2* as an internal control. **(F)** Glucose consumption and lactate production of hADMPCs were measured and plotted as the means of three independent experiments ± SD. **(G)** hADMPCs were transduced with either scrambled control RNAi (Cont) or RNAi against HES1 (HES1-KD), and then cultured for 3 days. Glucose consumption and lactate production of hADMPCs were measured and plotted as the means of three independent experiments ± SD. $^{**}P < 0.01$. $^{*}0.01 < P < 0.05$.

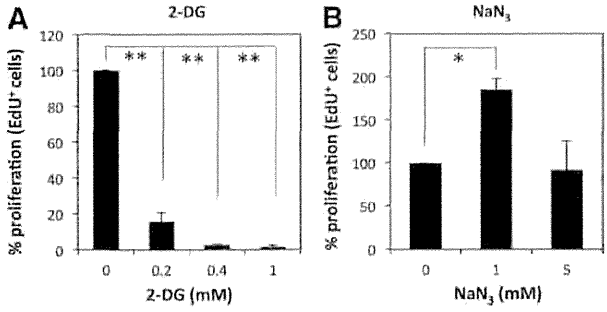

FIG. 7. Glycolysis supports proliferation of hADMPCs. hADMPCs were treated with 0, 0.2, 0.4, and 1 mM 2-deoxy-D-glucose (2-DG) **(A)** or 0, 1, and 5 mM sodium azide (NaN_3) **(B)** for 24 h. Cells were then allowed to incorporate EdU for 2 h, and the EdU-positive cells were analyzed by flow cytometry. The percentages for the 0 mM control were plotted as the means of three independent experiments ± SD. $*P < 0.05$; $**P < 0.01$.

modulator of aerobic respiration, and TIGAR, a negative regulator of glycolysis, were transcriptionally downregulated in the 5% oxygen condition; whereas DAPT treatment partially restored the expression level (Fig. 6B). Adenoviral expression of Hes1 dramatically reduced *SCO2* and *TIGAR* expression (Fig. 6E), which suggests that the Notch-Hes1 signaling modulates the metabolic pathway. We also measured the activities of key enzymes in glycolysis. Hexokinase activity was not changed under hypoxic conditions; however, PFK and LDH were activated in 5% oxygen condition, which was attenuated by Notch inhibition (Fig. 6C). In addition, pyruvate dehydrogenase (PDH) and cytochrome c oxidase (Complex IV) activity assays showed that mitochondrial respiration decreased under the hypoxic condition and that DAPT treatment restored it (Fig. 6D). Moreover, glycolytic flux in Hes1-expressing hADMPCs was positively correlated with the expression of these glycolytic genes as assessed by glucose consumption and lactate production (Fig. 6F). In contrast, HES1 knockdown by adenoviral transduction of *HES1* RNAi resulted in a significant reduction of glycolytic flux (Fig. 6G), demonstrating that HES1 is involved in the regulation of glycolysis.

Glycolysis supports the proliferation of hADMPCs

To determine whether aerobic glycolysis is important for the proliferation of hADMPCs, hADMPCs were treated with the glycolytic inhibitor 2-deoxy-D-glucose (2-DG) or the respiration inhibitor sodium azide (NaN_3). We found that hADMPCs were sensitive to treatment with 2-DG even at a low concentration of 0.2 mM (Fig. 7A). In contrast, treatment of hADMPCs with NaN_3 rather increased their proliferation at the concentration of 1 mM and supported their proliferation even at the concentration of 5 mM (Fig. 7B). These data suggest that the proliferation of hADMPCs is compromised when aerobic glycolysis is blocked.

Discussion

Recent evidence suggests that hypoxic culture conditions confer a growth advantage, prevent premature senescence, and maintain undifferentiated states in ESCs, iPSCs, and somatic stem cells. However, the molecular mechanism underlying the beneficial effects of culturing these cells at low oxygen conditions remains unclear. Our findings prompted us to hypothesize that Notch signaling in physiological hypoxic conditions (5% O_2) contributes to these effects on hADMPCs by modulating glycolytic flux.

We found that 5% O_2 significantly increased the proliferation capacity, decreased apoptosis, and inhibited senescence of hADMPCs (Fig. 1). Moreover, 5% O_2 improved the differentiation of hADMPCs without affecting the expression of their cell surface markers (Figs. 2 and 3). Welford et al. reported that HIF-1α delays premature senescence of mouse embryonic fibroblasts under hypoxic conditions (2% O_2) [50]. Tsai et al. reported that hypoxia (1% O_2) inhibits senescence and maintains MSC properties through accumulation of HIF-1α [26]. Hypoxia was recently reported to enhance the undifferentiated status and stem cell properties in various stem and precursor cell populations via the interaction of HIF with the Notch intracellular domain to activate Notch-responsive promoters [38]. In the current study, the effects observed in 5% O_2 condition were independent of HIF proteins, because accumulation of HIF-1α and HIF-2α was not observed (Fig. 4). Instead, our findings suggest that 5% O_2 activated Notch signaling, which contributed advantageous effects of hypoxic culture on hADMPCs. A pharmacological inhibitor of Notch signaling, DAPT, abrogated the hypoxic-induced Notch activation, increased proliferation capacity and lifespan, maintenance of stem cell properties, and prevention of senescence (Figs. 4 and 5). Moreover, we also found that 5% O_2 enhanced glucose consumption and lactate production, and these effects were also attenuated by Notch inhibition (Fig. 6A) and knockdown of HES1 (Fig. 6G). Previously, it has been reported that Notch signaling promotes glycolysis by activating the PI(3)K-Akt pathway [48,49]. However, our results indicate that Akt signaling was not activated by Notch signaling, because DAPT did not attenuate hypoxia-induced Akt phosphorylation (Fig. 4F). Although Akt is unlikely to be regulated by Notch signaling in hADMPCs, it is obvious in our data that Akt signaling was activated by 5% O_2. Therefore, we could not rule out the possibility that the promotion of glycolysis in the 5% O_2 condition was caused by Akt signaling.

Recent evidence suggests that Notch signaling acts as a metabolic switch [48,51]. Zhou et al. demonstrated that hairy, a basic helix-loop-helix transcriptional repressor regulated by Notch signaling, was upregulated and genes encoding metabolic enzymes, including TCA cycle enzymes and respiratory chain complexes, were downregulated in hypoxia-tolerant flies. Intriguingly, they also found that hairy-binding elements were present in the regulatory region of the downregulated metabolic genes. Their work, thus, provides new evidence that hairy acts as a metabolic switch [51]. Landor et al. demonstrated that both hyper- and hypoactive Notch signaling induced glycolysis, albeit by different mechanisms. They showed that Notch activation increased glycolysis through activation of PI3K-AKT signaling, whereas decreased Notch activity inhibited mitochondrial function in a p53-dependent manner in MCF7 breast cancer cell lines [48]. Consistent with their reports, our findings that Notch signaling promoted activity of some glycolysis enzymes and inhibited mitochondrial activity

(Fig. 6) also suggest that Notch signaling functioned as a metabolic switch. While our data showed that Notch inhibition by DAPT resulted in reduced glycolysis (Fig. 6A–C), induction of mitochondrial function (Fig. 6D) and activation of p53 (Fig. 4H, I) are not consistent with the report of Landor el al. This contradiction might be explained by the expression level of endogenous Notch. Landor et al. showed that in breast cancer MDA-M-231 cells, which showed higher endogenous Notch activity, high glucose uptake, and lactate production than MCF7 breast cancer cell lines, Notch inhibition by DAPT significantly reduced glucose consumption and lactate production [48]. As shown in Fig. 4A, we observed that hADMPCs in 5% O_2 displayed high Notch activity. Moreover, the lactate-to-glucose ratio was 1.8–1.9 in hADMPCs, suggesting that hADMPCs largely rely on glycolysis for energy production (Fig. 6A). In addition, it was reported that hMSCs showed a higher glycolytic rate than primary human fibroblast [52]. It appears that hADMPCs cultured under hypoxic conditions might possess cell properties similar to MDA-M-231 cells or MCF7 cells, in which stable expression of constructs NICD1-GFP produces high Notch activity.

Nuclear translocation of p65 was observed in hypoxic conditions, demonstrating that NF-κB is a direct target of Notch signaling (Fig. 4G). Intriguingly, the hypoxic culture conditions in this study upregulated several genes encoding glycolytic enzymes (*SLC2A3, TPI, and PGK1*); whereas the expression of these genes was suppressed by Notch inhibition. In addition, Hes1 transduction induced mRNA expression of the same genes (Fig. 6). It was previously reported that *SLC2A3* expression was regulated by p65/NF-κB signaling, and that Notch/Hes1 is able to induce the activation of the NF-κB pathway in human T-ALL lines and animal disease models [53]. Espinosa et al. demonstrated that Hes1 directly targeted the deubiquitinase CYLD, resulting in deubiquitination and inactivation of TAK1 and IKK, degradation of IκBa, and activation of NF-κB signaling [53]. In our systems, however, we did not observe repression of *CYLD* mRNA in Hes1-overexpressing hADMPCs (data not shown). While *PGK1* mRNA has been reported to be upregulated by NF-κB, it has not clearly been shown to be controlled by NF-κB despite the presence of an NF-κB site in the promoter [54]. Although modulation of *TPI* expression by NF-κB has not been reported, we found several NF-κB binding sites on the human *TPI* promoter (data not shown). Since NF-κB is likely to be one of the responsible signals for hypoxic-induced glycolysis [53], further analysis will be required to determine the mechanism by which NF-κB signaling is induced by Notch signaling. In addition, it will be important to investigate whether NF-κB is really responsible for the observed glycolysis and whether it regulates the expression of *SLC2A3*, *TPI*, and *PGK1* in hADMPCs under 5% oxygen.

In addition, SCO2, a positive modulator of aerobic respiration, and TIGAR, a negative regulator of glycolysis, were transcriptionally downregulated in the 5% oxygen condition; whereas DAPT treatment partially restored expression (Fig. 6B). We observed some glycolysis and mitochondrial enzyme activity and found that the activities of COX IV and PFK were consistent with gene expression data (Fig. 6C, D). Adenoviral expression of Hes1 dramatically reduced *SCO2* and *TIGAR* expression (Fig. 6E), which suggests that Notch-Hes1 signaling modulates the metabolic pathway. Intriguingly, our results also indicate that Hes1 could suppress the expression of *TIGAR* and *SCO2*, a p53 target gene. It has been reported that Notch signaling suppresses p53 in lymphomagenesis [46]. Moreover, Kim et al. reported that NICD1 inhibits p53 phosphorylation and represses p53 transactivation by interacting with p53 [47]. In addition, DAPT treatment resulted in the enhancement of p53 activity in the hypoxic conditions (Fig. 4H, I). Therefore, it is possible that p53 activation was regulated by Notch signaling in hADMPCs, although we did not observe a decrease in p53 activity in hypoxic conditions in this study (Fig. 4). Further analysis will be required to determine whether p53 activity is suppressed in hypoxic conditions over a longer period of culture.

Cells undergoing active proliferation utilize large amounts of glucose through glycolysis, producing pyruvate for use in substrates (amino acids and lipids) and the pentose shunt for use in nucleic acid substrates, and also producing NADPH as a reducing agent to counter oxidative stress [18,55]. In the current study, 5% O_2 actually increased proliferation and decreased the accumulation of ROS, which may be involved in the reduction of senescence (Fig. 1). Since accumulation of endogenous ROS might be a major reason for replicative senescence [20], enhancing glycolysis in cultured cells may improve the quality of the cells by suppressing premature senescence. Kondoh et al. demonstrated that enhanced glycolysis is involved in cellular immortalization through reduction of intrinsic ROS production [14,18,19]. Therefore, it is possible that the extension of lifespan observed in our experimental conditions was caused by the reduction of intracellular ROS levels through enhanced glycolysis by Notch signaling. Our data indicate that aerobic glycolysis is utilized for proliferation of hADMPCs, because the glycolytic inhibitor 2-DG attenuates the proliferation rate of hADMPCs (Fig. 7A). Intriguingly, the aerobic respiration block by NaN_3 did not decrease the proliferation; rather, it increased proliferation at a low concentration (Fig. 7B), which may support our data indicating that the metabolic switch from mitochondrial respiration to glycolysis provides a growth advantage to hADMPCs. However, the question of whether the enhanced glycolysis really contributes to the prolonged lifespan in hADMPCs remains to be determined in this study.

In the current study, the molecular mechanism for how Notch signaling is activated in 5% O_2 conditions was explored. It has been reported that Notch1 activity is influenced by oxygen concentration [40,41,56]. In melanoma cells, hypoxia (2% O_2) resulted in increased expression of Notch1 by HIF-1α and also by Akt through NF-κB activity [41]. Similarly, in hypoxic breast cancer cells, Notch ligand JAG2 was shown to be transcriptionally activated by hypoxia (1% O_2) in an HIF-1α-dependent manner, resulting in an elevation of Notch signaling [40]. In contrast, in hESCs continuously cultured in 5% O_2, alteration of the Notch pathway seems to be independent of HIF-1α [56]. In our system, Notch1 activation was not likely dependent on HIF-1α and HIF-2α, because these proteins did not accumulate in the Hx condition. In contrast, our results indicate that the 5% O_2 condition activated Akt and NF-κB signaling (Fig. 4), which suggests that these molecules may activate Notch signaling in hADMPCs. NF-κB was previously shown to

increase Notch1 activity indirectly by increasing the expression of Notch ligand Jagged1 in HeLa, lymphoma, and myeloma cells [57]. In addition, Akt regulated Notch1 by increasing Notch1 transcription through the activity of NF-κB in melanoma cells [41]. Further analysis is required to clarify the mechanism underlying this phenomenon.

In conclusion, the 5% oxygen condition conferred a growth advantage through a metabolic shift to glycolysis, improved the proliferation efficiency, prevented the cellular senescence, and maintained the undifferentiated status of hADMPCs. These observations, thus, provide new regulatory mechanisms for the maintenance of stemness observed in 5% oxygen conditions. In addition, our study sheds new light on the regulation of replicative senescence, which might have an impact for quality control of hADMPC preparations used for therapeutic applications.

Acknowledgments

The authors would like to thank Koichi Sakaguchi, Mio Oishi, Mika Uemura, and Kei Sawaragi for technical support. This work was supported by MEXT KAKENHI grant number 24791927 to H.M. This work was also supported in part by grants from the Ministry of Health, Labor, and Welfare of Japan and a grant from the Program for Promotion of Fundamental Studies in Health Sciences of the National Institute of Biomedical Innovation (NIBIO).

Author Disclosure Statement

The authors declare no conflict of interest. No competing financial interests exist.

References

1. Okura H, H Komoda, A Saga, A Kakuta-Yamamoto, Y Hamada, Y Fumimoto, CM Lee, A Ichinose, Y Sawa and A Matsuyama. (2010). Properties of hepatocyte-like cell clusters from human adipose tissue-derived mesenchymal stem cells. Tissue Eng Part C Methods 16:761–770.
2. Okura H, A Matsuyama, CM Lee, A Saga, A Kakuta-Yamamoto, A Nagao, N Sougawa, N Sekiya, K Takekita, et al. (2010). Cardiomyoblast-like cells differentiated from human adipose tissue-derived mesenchymal stem cells improve left ventricular dysfunction and survival in a rat myocardial infarction model. Tissue Eng Part C Methods 16:417–425.
3. Okura H, H Komoda, Y Fumimoto, CM Lee, T Nishida, Y Sawa and A Matsuyama. (2009). Transdifferentiation of human adipose tissue-derived stromal cells into insulin-producing clusters. J Artif Organs 12:123–130.
4. Safford KM, SD Safford, JM Gimble, AK Shetty and HE Rice. (2004). Characterization of neuronal/glial differentiation of murine adipose-derived adult stromal cells. Exp Neurol 187:319–328.
5. Leu S, YC Lin, CM Yuen, CH Yen, YH Kao, CK Sun and HK Yip. (2010). Adipose-derived mesenchymal stem cells markedly attenuate brain infarct size and improve neurological function in rats. J Transl Med 8:63.
6. Ikegame Y, K Yamashita, S Hayashi, H Mizuno, M Tawada, F You, K Yamada, Y Tanaka, Y Egashira, et al. (2011). Comparison of mesenchymal stem cells from adipose tissue and bone marrow for ischemic stroke therapy. Cytotherapy 13:675–685.
7. Tan B, Z Luan, X Wei, Y He, G Wei, BH Johnstone, M Farlow and Y Du. (2011). AMP-activated kinase mediates adipose stem cell-stimulated neuritogenesis of PC12 cells. Neuroscience 181:40–47.
8. Reid AJ, M Sun, M Wiberg, S Downes, G Terenghi and PJ Kingham. (2011). Nerve repair with adipose-derived stem cells protects dorsal root ganglia neurons from apoptosis. Neuroscience 199:515–522.
9. Rehman J, D Traktuev, J Li, S Merfeld-Clauss, CJ Temm-Grove, JE Bovenkerk, CL Pell, BH Johnstone, RV Considine and KL March. (2004). Secretion of angiogenic and antiapoptotic factors by human adipose stromal cells. Circulation 109:1292–1298.
10. Lee EY, Y Xia, WS Kim, MH Kim, TH Kim, KJ Kim, BS Park and JH Sung. (2009). Hypoxia-enhanced wound-healing function of adipose-derived stem cells: increase in stem cell proliferation and up-regulation of VEGF and bFGF. Wound Repair Regen 17:540–547.
11. Moriyama M, H Moriyama, A Ueda, Y Nishibata, H Okura, A Ichinose, A Matsuyama and T Hayakawa. (2012). Human adipose tissue-derived multilineage progenitor cells exposed to oxidative stress induce neurite outgrowth in PC12 cells through p38 MAPK signaling. BMC Cell Biol 13:21.
12. Wu H, Z Ye and RI Mahato. (2011). Genetically modified mesenchymal stem cells for improved islet transplantation. Mol Pharm 8:1458–1470.
13. Wagner W, P Horn, M Castoldi, A Diehlmann, S Bork, R Saffrich, V Benes, J Blake, S Pfister, V Eckstein and AD Ho. (2008). Replicative senescence of mesenchymal stem cells: a continuous and organized process. PLoS One 3: e2213.
14. Kondoh H, ME Lleonart, Y Nakashima, M Yokode, M Tanaka, D Bernard, J Gil and D Beach. (2007). A high glycolytic flux supports the proliferative potential of murine embryonic stem cells. Antioxid Redox Signal 9:293–299.
15. Prigione A, B Fauler, R Lurz, H Lehrach and J Adjaye. (2010). The senescence-related mitochondrial/oxidative stress pathway is repressed in human induced pluripotent stem cells. Stem Cells 28:721–733.
16. Varum S, AS Rodrigues, MB Moura, O Momcilovic, C At Easley, J Ramalho-Santos, B Van Houten and G Schatten. (2011). Energy metabolism in human pluripotent stem cells and their differentiated counterparts. PLoS One 6:e20914.
17. Warburg O, F Wind and E Negelein. (1927). The Metabolism of tumors in the body. J Gen Physiol 8:519–530.
18. Kondoh H. (2008). Cellular life span and the Warburg effect. Exp Cell Res 314:1923–1928.
19. Kondoh H, ME Lleonart, J Gil, J Wang, P Degan, G Peters, D Martinez, A Carnero and D Beach. (2005). Glycolytic enzymes can modulate cellular life span. Cancer Res 65: 177–185.
20. Beckman KB and BN Ames. (1998). The free radical theory of aging matures. Physiol Rev 78:547–581.
21. Ezashi T, P Das and RM Roberts. (2005). Low O2 tensions and the prevention of differentiation of hES cells. Proc Natl Acad Sci U S A 102:4783–4788.
22. Forristal CE, KL Wright, NA Hanley, RO Oreffo and FD Houghton. (2010). Hypoxia inducible factors regulate pluripotency and proliferation in human embryonic stem cells cultured at reduced oxygen tensions. Reproduction 139:85–97.
23. Yoshida Y, K Takahashi, K Okita, T Ichisaka and S Yamanaka. (2009). Hypoxia enhances the generation of induced pluripotent stem cells. Cell Stem Cell 5:237–241.

24. Takubo K, N Goda, W Yamada, H Iriuchishima, E Ikeda, Y Kubota, H Shima, RS Johnson, A Hirao, M Suematsu and T Suda. (2010). Regulation of the HIF-1alpha level is essential for hematopoietic stem cells. Cell Stem Cell 7:391–402.
25. Santilli G, G Lamorte, L Carlessi, D Ferrari, L Rota Nodari, E Binda, D Delia, AL Vescovi and L De Filippis. (2010). Mild hypoxia enhances proliferation and multipotency of human neural stem cells. PLoS One 5:e8575.
26. Tsai CC, YJ Chen, TL Yew, LL Chen, JY Wang, CH Chiu and SC Hung. (2011). Hypoxia inhibits senescence and maintains mesenchymal stem cell properties through down-regulation of E2A-p21 by HIF-TWIST. Blood 117: 459–469.
27. Takubo K, G Nagamatsu, CI Kobayashi, A Nakamura-Ishizu, H Kobayashi, E Ikeda, N Goda, Y Rahimi, RS Johnson, et al. (2013). Regulation of glycolysis by pdk functions as a metabolic checkpoint for cell cycle quiescence in hematopoietic stem cells. Cell Stem Cell 12: 49–61.
28. Grayson WL, F Zhao, R Izadpanah, B Bunnell and T Ma. (2006). Effects of hypoxia on human mesenchymal stem cell expansion and plasticity in 3D constructs. J Cell Physiol 207:331–339.
29. Wang DW, B Fermor, JM Gimble, HA Awad and F Guilak. (2005). Influence of oxygen on the proliferation and metabolism of adipose derived adult stem cells. J Cell Physiol 204:184–191.
30. Moriyama M, M Osawa, SS Mak, T Ohtsuka, N Yamamoto, H Han, V Delmas, R Kageyama, F Beermann, L Larue and S Nishikawa. (2006). Notch signaling via Hes1 transcription factor maintains survival of melanoblasts and melanocyte stem cells. J Cell Biol 173:333–339.
31. Chiba S. (2006). Notch signaling in stem cell systems. Stem Cells 24:2437–2447.
32. Okura H, A Saga, Y Fumimoto, M Soeda, M Moriyama, H Moriyama, K Nagai, CM Lee, S Yamashita, et al. (2011). Transplantation of human adipose tissue-derived multilineage progenitor cells reduces serum cholesterol in hyperlipidemic Watanabe rabbits. Tissue Eng Part C Methods 17:145–154.
33. Saga A, H Okura, M Soeda, J Tani, Y Fumimoto, H Komoda, M Moriyama, H Moriyama, S Yamashita, et al. (2011). HMG-CoA reductase inhibitor augments the serum total cholesterol-lowering effect of human adipose tissue-derived multilineage progenitor cells in hyperlipidemic homozygous Watanabe rabbits. Biochem Biophys Res Commun 412:50–54.
34. Moriyama H, M Moriyama, K Sawaragi, H Okura, A Ichinose, A Matsuyama and T Hayakawa. (2013). Tightly regulated and homogeneous transgene expression in human adipose-derived mesenchymal stem cells by lentivirus with tet-off system. PLoS One 8:e66274.
35. Sekiya I, BL Larson, JR Smith, R Pochampally, JG Cui and DJ Prockop. (2002). Expansion of human adult stem cells from bone marrow stroma: conditions that maximize the yields of early progenitors and evaluate their quality. Stem Cells 20:530–541.
36. Wagner W, F Wein, A Seckinger, M Frankhauser, U Wirkner, U Krause, J Blake, C Schwager, V Eckstein, W Ansorge and AD Ho. (2005). Comparative characteristics of mesenchymal stem cells from human bone marrow, adipose tissue, and umbilical cord blood. Exp Hematol 33:1402–1416.
37. Hass R, C Kasper, S Bohm and R Jacobs. (2011). Different populations and sources of human mesenchymal stem cells (MSC): A comparison of adult and neonatal tissue-derived MSC. Cell Commun Signal 9:12.
38. Gustafsson MV, X Zheng, T Pereira, K Gradin, S Jin, J Lundkvist, JL Ruas, L Poellinger, U Lendahl and M Bondesson. (2005). Hypoxia requires notch signaling to maintain the undifferentiated cell state. Dev Cell 9:617–628.
39. Zheng X, S Linke, JM Dias, X Zheng, K Gradin, TP Wallis, BR Hamilton, M Gustafsson, JL Ruas, et al. (2008). Interaction with factor inhibiting HIF-1 defines an additional mode of cross-coupling between the Notch and hypoxia signaling pathways. Proc Natl Acad Sci U S A 105:3368–3373.
40. Pietras A, K von Stedingk, D Lindgren, S Pahlman and H Axelson. (2011). JAG2 induction in hypoxic tumor cells alters Notch signaling and enhances endothelial cell tube formation. Mol Cancer Res 9:626–636.
41. Bedogni B, JA Warneke, BJ Nickoloff, AJ Giaccia and MB Powell. (2008). Notch1 is an effector of Akt and hypoxia in melanoma development. J Clin Invest 118:3660–3670.
42. Beitner-Johnson D, RT Rust, TC Hsieh and DE Millhorn. (2001). Hypoxia activates Akt and induces phosphorylation of GSK-3 in PC12 cells. Cell Signal 13:23–27.
43. Culver C, A Sundqvist, S Mudie, A Melvin, D Xirodimas and S Rocha. (2010). Mechanism of hypoxia-induced NF-kappaB. Mol Cell Biol 30:4901–4921.
44. Rohwer N, C Dame, A Haugstetter, B Wiedenmann, K Detjen, CA Schmitt and T Cramer. (2010). Hypoxia-inducible factor 1alpha determines gastric cancer chemosensitivity via modulation of p53 and NF-kappaB. PLoS One 5:e12038.
45. Espinosa L, S Cathelin, T D'Altri, T Trimarchi, A Statnikov, J Guiu, V Rodilla, J Ingles-Esteve, J Nomdedeu, et al. (2010). The Notch/Hes1 pathway sustains NF-kappaB activation through CYLD repression in T cell leukemia. Cancer Cell 18:268–281.
46. Beverly LJ, DW Felsher and AJ Capobianco. (2005). Suppression of p53 by Notch in lymphomagenesis: implications for initiation and regression. Cancer Res 65:7159–7168.
47. Kim SB, GW Chae, J Lee, J Park, H Tak, JH Chung, TG Park, JK Ahn and CO Joe. (2007). Activated Notch1 interacts with p53 to inhibit its phosphorylation and transactivation. Cell Death Differ 14:982–991.
48. Landor SK, AP Mutvei, V Mamaeva, S Jin, M Busk, R Borra, TJ Gronroos, P Kronqvist, U Lendahl and CM Sahlgren. (2011). Hypo- and hyperactivated Notch signaling induce a glycolytic switch through distinct mechanisms. Proc Natl Acad Sci U S A 108:18814–18819.
49. Ciofani M and JC Zuniga-Pflucker. (2005). Notch promotes survival of pre-T cells at the beta-selection checkpoint by regulating cellular metabolism. Nat Immunol 6: 881–888.
50. Welford SM, B Bedogni, K Gradin, L Poellinger, M Broome Powell and AJ Giaccia. (2006). HIF1alpha delays premature senescence through the activation of MIF. Genes Dev 20:3366–3371.
51. Zhou D, J Xue, JC Lai, NJ Schork, KP White and GG Haddad. (2008). Mechanisms underlying hypoxia tolerance in Drosophila melanogaster: hairy as a metabolic switch. PLoS Genet 4:e1000221.
52. Funes JM, M Quintero, S Henderson, D Martinez, U Qureshi, C Westwood, MO Clements, D Bourboulia, RB Pedley,

S Moncada and C Boshoff. (2007). Transformation of human mesenchymal stem cells increases their dependency on oxidative phosphorylation for energy production. Proc Natl Acad Sci U S A 104:6223–6228.
53. Kawauchi K, K Araki, K Tobiume and N Tanaka. (2008). p53 regulates glucose metabolism through an IKK-NF-kappaB pathway and inhibits cell transformation. Nat Cell Biol 10:611–618.
54. Carter KL, E Cahir-McFarland and E Kieff. (2002). Epstein-barr virus-induced changes in B-lymphocyte gene expression. J Virol 76:10427–10436.
55. Ak P and AJ Levine. (2010). p53 and NF-kappaB: different strategies for responding to stress lead to a functional antagonism. FASEB J 24:3643–3652.
56. Prasad SM, M Czepiel, C Cetinkaya, K Smigielska, SC Weli, H Lysdahl, A Gabrielsen, K Petersen, N Ehlers, et al. (2009). Continuous hypoxic culturing maintains activation of Notch and allows long-term propagation of human embryonic stem cells without spontaneous differentiation. Cell Prolif 42:63–74.
57. Bash J, WX Zong, S Banga, A Rivera, DW Ballard, Y Ron and C Gelinas. (1999). Rel/NF-kappaB can trigger the Notch signaling pathway by inducing the expression of Jagged1, a ligand for Notch receptors. EMBO J 18:2803–2811.

Address correspondence to:
Dr. Hiroyuki Moriyama
Pharmaceutical Research and Technology Institute
Kinki University
3-4-1 Kowakae
Higashi-Osaka
Osaka 577-8502
Japan

E-mail: moriyama@phar.kindai.ac.jp

Received for publication December 26, 2013
Accepted after revision May 15, 2014
Prepublished on Liebert Instant Online May 30, 2014

Biologicals 43 (2015) 146–149

Contents lists available at ScienceDirect

Biologicals

journal homepage: www.elsevier.com/locate/biologicals

Short paper

Characterization of the cell growth analysis for detection of immortal cellular impurities in human mesenchymal stem cells

Ken Kono [a, 1], Nozomi Takada [b, c, 1], Satoshi Yasuda [b, d], Rumi Sawada [a], Shingo Niimi [a], Akifumi Matsuyama [c], Yoji Sato [b, d, e, f, g, *]

[a] Division of Medical Devices, National Institute of Health Sciences, 1-18-1 Kami-yoga, Setagaya, Tokyo 158-8501, Japan
[b] Division of Cellular & Gene Therapy Products, National Institute of Health Sciences, 1-18-1 Kami-yoga, Setagaya, Tokyo 158-8501, Japan
[c] Research on Disease Bioresources, Platform of Therapeutics for Rare Disease and Health Policy, National Institute of Biomedical Innovation, Kobe International Business Center Rm#602, 5-5-2 Minatojima-Minami-Machi, Chuo-ku, Kobe, Hyogo 650-0047, Japan
[d] Foundation for Biomedical Research and Innovation, Hyogo, Japan
[e] Department of Quality Assurance Science for Pharmaceuticals, Graduate School of Pharmaceutical Sciences, Nagoya City University, Aichi, Japan
[f] Department of Cellular & Gene Therapy Products, Graduate School of Pharmaceutical Sciences, Osaka University, Osaka, Japan
[g] Department of Translational Pharmaceutical Sciences, Graduated School of Pharmaceutical Sciences, Kyushu University, Fukuoka, Japan

ARTICLE INFO

Article history:
Received 1 October 2014
Received in revised form
13 November 2014
Accepted 24 November 2014
Available online 16 December 2014

Keywords:
Regenerative medicine
Cellular therapy
Tumorigenicity
Mesenchymal stem cell
Quality
Safety

ABSTRACT

The analysis of *in vitro* cell senescence/growth after serial passaging can be one of ways to show the absence of immortalized cells, which are frequently tumorigenic, in human cell-processed therapeutic products (hCTPs). However, the performance of the cell growth analysis for detection of the immortalized cellular impurities has never been evaluated. In the present study, we examined the growth rates of human mesenchymal stem cells (hMSCs, passage 5 ($P = 5$)) contaminated with various doses of HeLa cells, and compared with that of hMSCs alone. The growth rates of the contaminated hMSCs were comparable to that of hMSCs alone at $P = 5$, but significantly increased at $P = 6$ (0.1% and 0.01% HeLa) or $P = 7$ (0.001% HeLa) within 30 days. These findings suggest that the cell growth analysis is a simple and sensitive method to detect immortalized cellular impurities in hCTPs derived from human somatic cells.

1. Introduction

Human cell-processed therapeutic products (hCTPs) are expected to provide novel breakthrough therapies for currently life-threatening or incurable diseases. In the clinical applications of hCTPs to patients, however, one of the major concerns is the tumorigenic cellular impurities in the products. Since pluripotent stem cells (PSCs), such as embryonic stem cells and induced pluripotent stem cells, are tumorigenic [1–3], there is a risk of tumor formation if the products contain the residual undifferentiated PSCs [4]. On the other hand, somatic cells are considered to have little tumorigenic potential even after substantial manipulations like *in vitro* expansion, because they consistently pass into senescence [5]. Malignant transformation of the cells is believed to occur through multiple processes involving the accumulation of mutations in key regulatory genes that promote cell survival and proliferation [6,7]. Although a few individual groups reported the spontaneous transformation of human mesenchymal stem cells (hMSCs) during *in vitro* culture [8–11], two of them retracted their papers because the results appeared to be attributable to contamination with tumorigenic cells (fibrosarcoma, osteosarcoma, or glioma cell lines) [12,13]. The rest of the groups found the immortalization of the cells, which is closely associated with tumorigenicity, during *in vitro* culture, indicating that the good practices to avoid contamination with tumorigenic cells and the monitoring of cell growth are critical for the quality control of hCTPs derived from human somatic cells.

* Corresponding author. Division of Cellular and Gene Therapy Products, National Institute of Health Sciences, 1-18-1 Kami-yoga, Setagaya, Tokyo 158-8501, Japan.
E-mail addresses: kenkono@nihs.go.jp (K. Kono), takada.n@nihs.go.jp (N. Takada), yasuda@nihs.go.jp (S. Yasuda), rsawada@nihs.go.jp (R. Sawada), niimi@nihs.go.jp (S. Niimi), akifumi-matsuyama@umin.ac.jp (A. Matsuyama), yoji@nihs.go.jp (Y. Sato).
[1] These authors contributed equally to this work.

http://dx.doi.org/10.1016/j.biologicals.2014.11.007

Abbreviations

hCTP	human cell-processed therapeutic product
PSC	pluripotent stem cell
hMSC	human mesenchymal stem cell
STR	short tandem repeat
$P = n$	passage n
PBS	phosphate buffered saline
RT	room temperature
HPV	human papillomavirus

Cross contamination of cells with unidentified cells is usually evaluated by the short tandem repeat (STR) analysis [14]. However, the cell growth analysis which simply monitors the cell proliferation for a limited period may be adequately sensitive for the detection of the contamination of somatic cells with immortalized/tumorigenic cells, because somatic cells usually show slower growth, compared with that of immortalized/tumorigenic cells, as well as the attenuation of the growth after serial passaging [15–17]. In fact, the European Medicines Agency has considered that the evaluation of *in vitro* cell senescence after serial passaging is sufficient to prove the absence of immortalized/tumorigenic cells in a somatic cell-based product [18]. However, the performance of the cell growth analysis for detection of the immortalized/tumorigenic cellular impurities in somatic cells has never been studied. In the present study, we examined the growth of hMSCs contaminated with various doses of HeLa cells, a well-known cancer cell line, to determine the sensitivity of the cell growth analysis for the detection of the immortalized/tumorigenic cells in human somatic cells.

2. Materials and methods

2.1. Cells

hMSCs (Lonza, Walkersville, MD) at passage 2 ($P = 2$) were cultured in MSCGM BulletKit, a mesenchymal stem cell basal medium with mesenchymal cell growth supplement, L-glutamine, and gentamycin/amphotericin-B (Lonza). HeLa cells (the Health Science Research Resources Bank, Osaka, Japan) were maintained in Eagle's minimum essential medium (Sigma), supplemented with 10% fetal bovine serum (FBS; Sigma), 0.1 mM non-essential amino acids (Life Technologies), 50 U/ml penicillin, and 50 μg/ml streptomycin (Life Technologies). Cells were cultured in a humidified atmosphere of 5% CO_2 and 95% air at 37 °C, and were passaged upon reaching 90% confluence.

2.2. Cell growth analysis

At $P = 5$ of hMSCs, 1×10^6 of hMSCs were mixed with 1000, 100, or 10 of HeLa cells and seeded into T175 flasks (Corning). The cells were maintained in 40 ml of Dulbecco's Modified Eagle's medium (DMEM; Gibco) supplemented with 10% FBS, 50 U/ml penicillin, and 50 μg/ml streptomycin. Upon reaching approximately 90% confluence, the cells were washed with phosphate buffered saline (PBS) and treated with 0.05% trypsin-EDTA solution (Gibco) for detachment from the flasks. The cells were centrifuged at 450 × *g* for 5 min and suspended with the fresh culture medium. Aliquots of the suspended cells were stained with Trypan Blue solution and counted by Countess Automated Cell Counter (Invitrogen) according to the manufacture's protocol. One million cells in the suspension were re-seeded into T175 flasks and cultured until the next passage. This process was repeated by $P = 10$. The growth rate (R_n) at $P = n$ was calculated by the following equation:

$$R_n = [\log_2(N_{n+1} - N_n)]/(D_{n+1} - D_n)$$

where N_k and D_k are the number of accumulated cells and the date at $P = k$, respectively.

2.3. Immunofluorescence microscopy

hMSCs contaminated with HeLa cells were fixed with 4% paraformaldehyde in PBS (Nacalai Tesque) for 10 min at room temperature (RT) and blocked in Blocking One (Nacalai Tesque) for 30 min at RT. The cells, then, were incubated with anti-HPV18 E7 antibody (8E2) (abcam) diluted at 1:500 in the blocking solution (PBS containing 5% Blocking One) for 1 h at RT for primary staining, and secondarily stained with goat anti-mouse IgG Alexa Fluor 488 (1:1000; Invitrogen) in the blocking solution for 45 min at RT. The cells were mounted with VECTASGIELD mounting medium with DAPI (VECTOR) and observed with a fluorescence microscope (IX71, Olympus).

3. Results and discussion

In the present study, we added 1000, 100, or 10 of HeLa cells to 1×10^6 of hMSCs of passage 5 ($P = 5$) and compared their growth with that of hMSCs alone (HeLa 0) until $P = 10$. The growth curves of three lots of hMSCs and the contaminated hMSCs are shown in Fig. 1. The cell numbers of HeLa 0 and the contaminated hMSCs were comparable at $P = 5$. The growth of HeLa 0 was constant during the early culture and getting slower with time (Fig. 1), while the growth of the contaminated cells was accelerated.

To confirm that the increases in the growth were attributable to the contamination with HeLa cells, we observed the cells with phase contrast microscopy. In the images of the contaminated hMSCs, we found small cells clearly different from hMSCs (Fig. 2A), and their relative abundance increased every passage. Because HeLa cells are infected with human papillomaviruses (HPV), we performed immunofluorescence analysis using HPV18 E7 antibody and confirmed that the cells were HeLa cells not transformed hMSCs (Fig. 2B). At $P = 10$, hMSCs were hardly identified in images of HeLa 1000 (Fig. 2C), because almost all of hMSCs were exchanged for HeLa cells at the five passages.

Next, we examined the growth rates of the contaminated cells (Fig. 3A). They were comparable to that of HeLa 0 at $P = 5$, and got significantly increased at $P = 6$ (HeLa 1000 and HeLa 100) or $P = 7$ (HeLa 10). These results indicated that the gross proliferation rate was not influenced by the spiked cells at $P = 5$ and then the population of HeLa cells in hMSCs increased in dose- and time-dependent manner. Eventually, the growth rate (doubling/day) of the contaminated hMSCs increased, and then reached plateau. The average growth rate of the contaminated cells at $P = 9$ and 10 was 0.73, suggesting that the growth rate of HeLa cells was approximately 0.7 in this culture condition. The average growth rates of the three lots are plotted along the passage number in Fig. 3B. The growth rates of HeLa 1000 and HeLa 100 at $P = 7$ and HeLa 10 at $P = 8$ were significantly increased compared with the growth rates at $P = 5$ ($^*P < 0.05$, two-way repeated measures ANOVA and Student-Newman–Keulis test). These results indicate that the cell cultures longer than $P = 7$ (about 20 days) and $P = 8$ (about 30 days) detect cross-contaminations of 100 (0.01%) and 10 (0.001%) HeLa cells, respectively, assuming that 10^6 hMSCs were contaminated at $P = 5$.

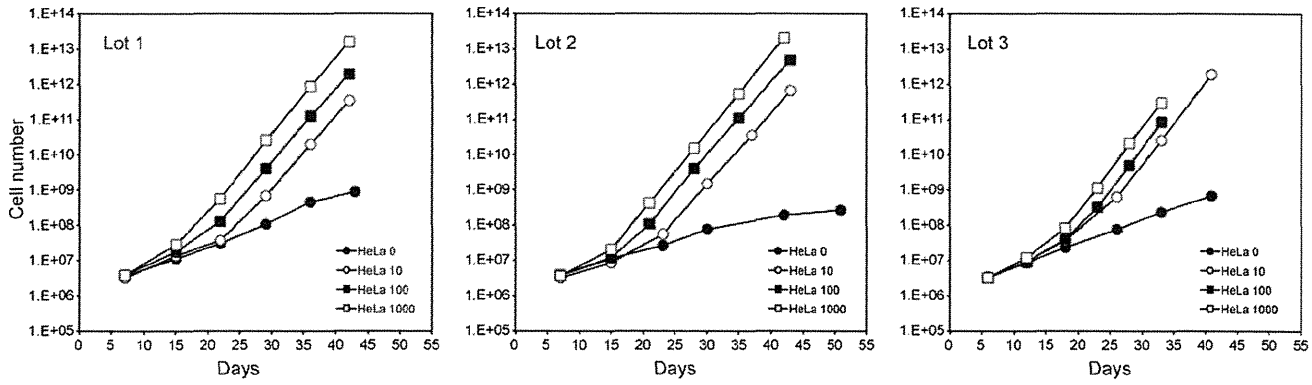

Fig. 1. Cell growth analysis of hMSCs contaminated with HeLa cells. At the passage 5 ($P = 5$) of hMSCs, 1×10^6 of hMSCs were mixed with 0, 10, 100, or 1000 of HeLa cells (HeLa 0, HeLa 10, HeLa 100, or HeLa 1000). Cells were passaged and counted at the indicated day from $P = 5$. The results of three lots of hMSCs are presented (Lot 1, 2, and 3).

The tumorigenicity has been evaluated by *in vitro* assays (e.g., soft agar formation assay, karyotype analysis) and/or *in vivo* assays (transplantation into immunodeficient animals) [8,9,19,20]. When these assays are performed to detect a trace amount of tumorigenic cells in hCTPs, they need to be of high sensitivity. Recently, we developed a highly sensitive *in vivo* tumorigenicity test using severely immunocompromised mice, NOG mice, in combination with Matrigel. Subcutaneous transplantation into NOG mice with Matrigel allowed inoculation with 1×10^7 cells and actually achieved detection of 0.002% HeLa cells spiked into hMSCs in a half of the mice (unpublished data). However, *in vivo* tumorigenicity test using immunodeficient animals requires a specific facility, and takes 3–4 months. In contrast, the cell growth analysis is not only simple and economical, but also detects as few as 0.001% immortal cellular impurities in hMSCs within 30 days, in case that the growth properties of the immortal cells are comparable to those of HeLa cells. Although immortality does not necessarily indicate tumorigenicity, it is known to be closely associated with cell transformation in many cases of tumorigenesis. Therefore, the present study can be said to be the first scientific basis for the usefulness of the cell growth analysis as one of tumorigenicity tests for hCTPs derived from human somatic cells.

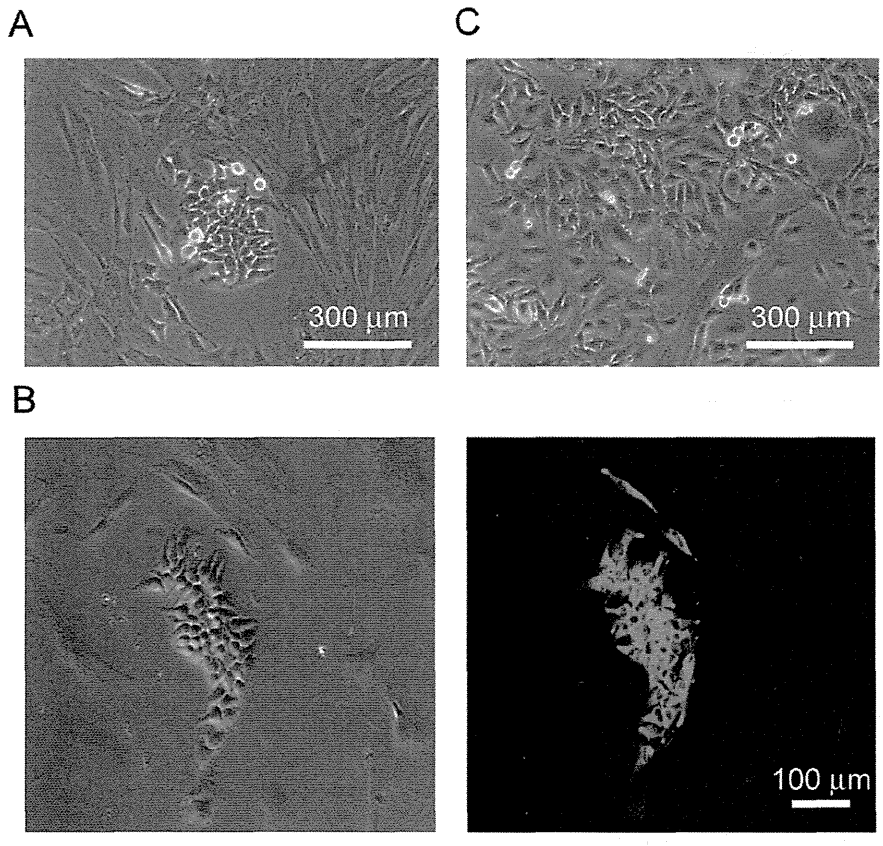

Fig. 2. Phase contrast and immunofluorescence microscopy of hMSCs contaminated with HeLa cells. (A) Representative image of the contaminated cells (HeLa 100 at $P = 8$) is presented. Red arrow pointed at the small size cells which were clearly different from hMSCs. (B) Phase contrast and immunofluorescence microscopy of HeLa 1000 at day 5 was conducted by using anti-HPV E7 antibody. Green: Alexa Fluor 488 goat anti-mouse IgG; blue: DAPI. (C) Representative image of HeLa 1000 at P10 is presented.

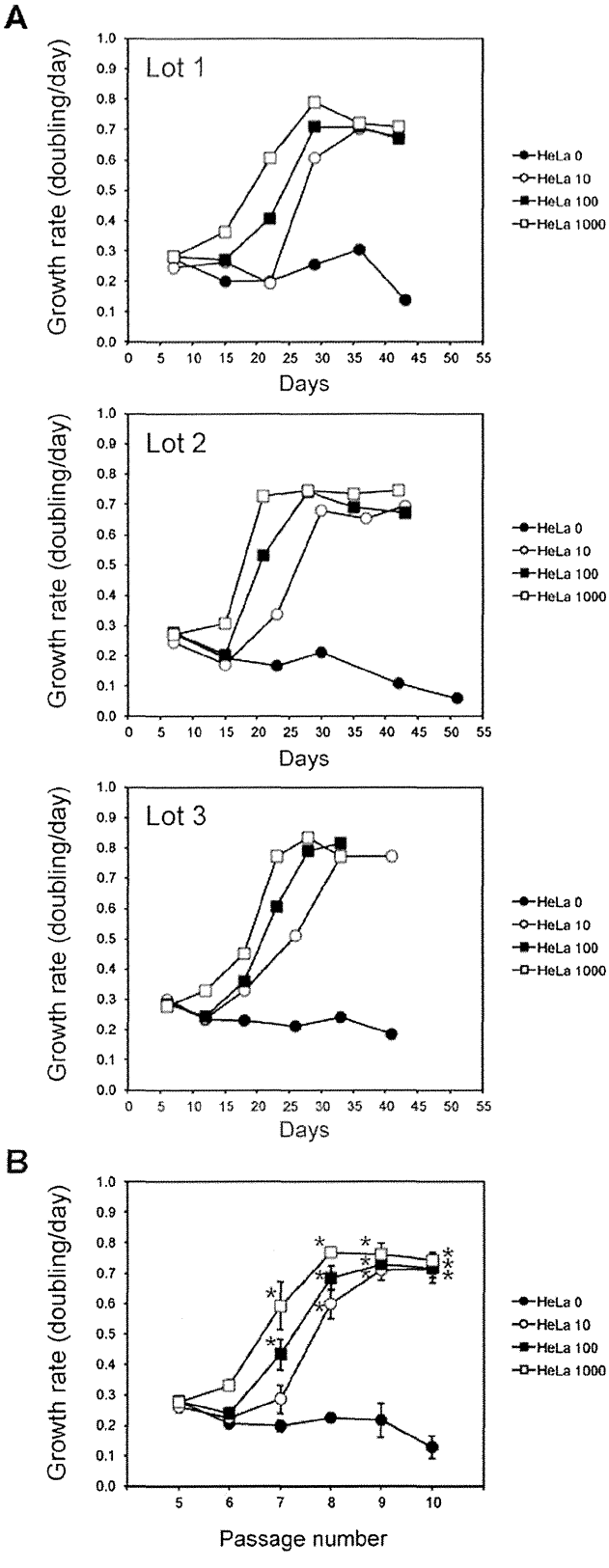

Fig. 3. Cell growth rate analysis of hMSCs contaminated with HeLa cells. (A) The *Y*-axis indicates the growth rate (doubling per day) of hMSCs. The results of three lots of hMSCs are presented (Lot 1, 2, and 3). (B) The growth rates of three lots of hMSCs are plotted along the passage numbers. Data are represented as mean ± S.E.M. of the three lots. Statistical significance was determined using two-way repeated measures ANOVA and Student-Newman–Keulis's post-hoc test (*$P < 0.05$ compared with the rate at $P = 5$).

Author contributions

Conceived and designed the experiments: KK NT SY RS YS. Performed the experiments: KK NT. Analyzed and Interpreted the data: KK NT SY RS SN AM YS. Contributed regents/materials/analysis tools: SN AM YS. Wrote the paper: KK NT SY YS. Acquired the funding: AM YS.

Competing interests

The authors have declared that no competing interests exist.

Acknowledgments

This work was supported by Research Grants from the Japanese Ministry of Health, Labour and Welfare (H23-SAISEI-IPPAN-005, H24-IYAKU-SHITEI-027, H25-JITSUYOKA(SAISEI)-IPPAN-008, and Marketing Authorization Facilitation Program for Innovative Therapeutic Products).

References

[1] Takahashi K, Tanabe K, Ohnuki M, Narita M, Ichisaka T, Tomoda K, et al. Induction of pluripotent stem cells from adult human fibroblasts by defined factors. Cell 2007;131:861–72.
[2] Thomson JA, Itskovitz-Eldor J, Shapiro SS, Waknitz MA, Swiergiel JJ, Marshall VS, et al. Embryonic stem cell lines derived from human blastocysts. Science 1998;282:1145–7.
[3] Yu J, Vodyanik MA, Smuga-Otto K, Antosiewicz-Bourget J, Frane JL, Tian S, et al. Induced pluripotent stem cell lines derived from human somatic cells. Science 2007;318:1917–20.
[4] Kuroda T, Yasuda S, Sato Y. Tumorigenicity studies for human pluripotent stem cell-derived products. Biol Pharm Bull 2013;36:189–92.
[5] Prockop DJ. Defining the probability that a cell therapy will produce a malignancy. Mol Ther 2010;18:1249–50.
[6] Vogelstein B, Kinzler KW. Cancer genes and the pathways they control. Nat Med 2004;10:789–99.
[7] Blagosklonny MV. Target for cancer therapy: proliferating cells or stem cells. Leukemia 2006;20:385–91.
[8] Rubio D, Garcia-Castro J, Martin MC, de la Fuente R, Cigudosa JC, Lloyd AC, et al. Spontaneous human adult stem cell transformation. Cancer Res 2005;65:3035–9.
[9] Rosland GV, Svendsen A, Torsvik A, Sobala E, McCormack E, Immervoll H, et al. Long-term cultures of bone marrow-derived human mesenchymal stem cells frequently undergo spontaneous malignant transformation. Cancer Res 2009;69:5331–9.
[10] Wang Y, Huso DL, Harrington J, Kellner J, Jeong DK, Turney J, et al. Outgrowth of a transformed cell population derived from normal human BM mesenchymal stem cell culture. Cytotherapy 2005;7:509–19.
[11] Tang DQ, Wang Q, Burkhardt BR, Litherland SA, Atkinson MA, Yang LJ. In vitro generation of functional insulin-producing cells from human bone marrow-derived stem cells, but long-term culture running risk of malignant transformation. Am J Stem Cells 2012;1:114–27.
[12] Torsvik A, Rosland GV, Svendsen A, Molven A, Immervoll H, McCormack E, et al. Spontaneous malignant transformation of human mesenchymal stem cells reflects cross-contamination: putting the research field on track – letter. Cancer Res 2010;70:6393–6.
[13] de la Fuente R, Bernad A, Garcia-Castro J, Martin MC, Cigudosa JC. Retraction: spontaneous human adult stem cell transformation. Cancer Res 2010;70:6682.
[14] Dirks WG, MacLeod RA, Nakamura Y, Kohara A, Reid Y, Milch H, et al. Cell line cross-contamination initiative: an interactive reference database of STR profiles covering common cancer cell lines. Int J Cancer 2010;126:303–4.
[15] Hayflick L, Moorhead PS. The serial cultivation of human diploid cell strains. Exp Cell Res 1961;25:585–621.
[16] Hayflick L. The cell biology of aging. Clin Geriatr Med 1985;1:15–27.
[17] Hayflick L. The limited in vitro lifetime of human diploid cell strains. Exp Cell Res 1965;37:614–36.
[18] European medicines Agency EMEA/724428/2009 assessment report for ChondroCelect. 2009.
[19] Kuroda T, Yasuda S, Kusakawa S, Hirata N, Kanda Y, Suzuki K, et al. Highly sensitive in vitro methods for detection of residual undifferentiated cells in retinal pigment epithelial cells derived from human iPS cells. PLoS One 2012;7:e37342.
[20] Rangarajan A, Hong SJ, Gifford A, Weinberg RA. Species- and cell type-specific requirements for cellular transformation. Cancer Cell 2004;6:171–83.

Regenerative Therapy 1 (2015) 30–37

Contents lists available at ScienceDirect

Regenerative Therapy

journal homepage: http://www.elsevier.com/locate/reth

Original article

Characterization of *in vivo* tumorigenicity tests using severe immunodeficient NOD/Shi-scid IL2Rγ^{null} mice for detection of tumorigenic cellular impurities in human cell-processed therapeutic products

Shinji Kusakawa [a, b], Kazuhiko Machida [c], Satoshi Yasuda [a, b], Nozomi Takada [a, d, 1], Takuya Kuroda [a, b], Rumi Sawada [a], Hanayuki Okura [d, 1], Hideki Tsutsumi [c], Shin Kawamata [b], Yoji Sato [a, b, e, f, g, *]

[a] Division of Cell-Based Therapeutic Products, National Institute of Health Sciences, Tokyo, Japan
[b] Foundation for Biomedical Research and Innovation, Kobe, Japan
[c] Testing Department, Central Institute for Experimental Animals, Kawasaki, Japan
[d] Platform for Realization of Regenerative Medicine, Foundation for Biomedical Research and Innovation, Kobe, Japan
[e] Department of Quality Assurance Science for Pharmaceuticals, Graduate School of Pharmaceutical Sciences, Nagoya City University, Nagoya, Japan
[f] Department of Cellular and Gene Therapy Products, Graduate School of Pharmaceutical Sciences, Osaka University, Osaka, Japan
[g] Department of Translational Pharmaceutical Sciences, Graduate School of Pharmaceutical Sciences, Kyushu University, Fukuoka, Japan

ARTICLE INFO

Article history:
Received 11 September 2014
Received in revised form
14 December 2014
Accepted 28 December 2014

Keywords:
Tumorigenicity test
NOG mice
Cellular therapy
Regenerative medicine
Quality control

ABSTRACT

The contamination of human cell-processed therapeutic products (hCTPs) with tumorigenic cells is one of the major concerns in the manufacturing and quality control of hCTPs. However, no quantitative method for detecting the tumorigenic cellular impurities is currently standardized. NOD/Shi-scid IL2Rγ^{null} (NOG) mice have shown high xeno-engraftment potential compared with other well-known immunodeficient strains, e.g. nude mice. Hypothesizing that tumorigenicity test using NOG mice could be a sensitive and quantitative method to detect a small amount of tumorigenic cells in hCTPs, we examined tumor formation after subcutaneous transplantation of HeLa cells, as a model of tumorigenic cells, in NOG mice and nude mice. Sixteen weeks after inoculation, the 50% tumor-producing dose (TPD_{50}) values of HeLa cells were stable at 1.3×10^4 and 4.0×10^5 cells in NOG and nude mice, respectively, indicating a 30-fold higher sensitivity of NOG mice compared to that of nude mice. Transplanting HeLa cells embedded with Matrigel in NOG mice further decreased the TPD_{50} value to 7.9×10 cells, leading to a 5000-fold higher sensitivity, compared with that of nude mice. Additionally, when HeLa cells were mixed with 10^6 or 10^7 human mesenchymal stem cells as well as Matrigel, the TPD_{50} values in NOG mice were comparable to those of HeLa cells alone with Matrigel. These results suggest that the *in vivo* tumorigenicity test using NOG mice with Matrigel is a highly sensitive and quantitative method to detect a trace amount of tumorigenic cellular impurities in human somatic cells, which can be useful in the quality assessment of hCTPs.

1. Introduction

Cell-processed therapeutic products (CTPs) derived from human somatic/stem cells are eagerly expected to treat patients with severe diseases involving functional damage of organs and tissues. To transplant hCTPs into patients, however, tumorigenicity is raised as one of the issues of these products. Tumorigenicity is defined as the capacity of a cell population transplanted into an animal model to

* Corresponding author. 1-18-1 Kamiyoga, Setagaya-ku, Tokyo 158-8501, Japan. Tel./fax: +81 3 3700 9373.
E-mail address: yoji@nihs.go.jp (Y. Sato).

Peer review under responsibility of the Japanese Society for Regenerative Medicine.

[1] Present address: Research on Disease Bioresources, Platform of Therapeutics for Rare Disease and Health Policy, National Institute of Biomedical Innovation, Kobe, Japan.

http://dx.doi.org/10.1016/j.reth.2014.12.001

produce a tumor by proliferation at the site of transplantation and/or at a distant site by metastasis [1]. Assessment of tumorigenicity is quite important to manufacture products with consistent quality. Currently, the World Health Organization (WHO) Technical Report Series (TRS) No. 878 Annex 1 is the only international guideline that addresses tumorigenicity tests of animal cells for the production of biologicals. However, the tumorigenicity test described in WHO TRS 878, which involves the administration of 10^7 cells to ten nude mice, would not be sensitive enough to detect a trace amount of tumorigenic cellular impurities in hCTPs [2]. In addition, the *in vivo* tumorigenicity test proposed in WHO TRS 878 covers only viable animal cells used as cell substrates for manufacturing biological products but not cells used directly for therapy by transplantation into patients. Thus, to date, no suitable tumorigenicity test has been established for hCTPs.

To establish methods to detect a trace amount of tumorigenic cellular impurities in hCTPs, the usage of several new generations of highly immunodeficient animal models are proposed. Rag2-γC double-knockout mice [3], NOD/Shi-scid IL2Rγ^{null} (NOG) mice [4], and NOD/SCID/IL-2rγKO (NSG) mice [5] indicate multiple immunodeficiencies, including defects in T, B, and natural killer (NK) cells, and a reduction in the function of macrophages and dendritic cells. NOG mice exhibit extremely high engraftment rates of human HeLa S3 cells compared with T-cell-deficient nude mice and T and B-cell-deficient SCID mice [6]. NSG mice are reported to show efficient tumor formation by single human melanoma cells in combination with Matrigel, a basement membrane-like extracellular matrix extract [7]. However, for the use of these highly immunodeficient mouse strains to detect tumorigenic cellular impurities in hCTPs as a part of the quality assessment/control, the performance of the tumorigenicity tests using these strains shall be validated using well known tumor cell lines.

In the present study, we examined the tumor formation potential of HeLa cells transplanted in NOG mice with Matrigel and compared their tumorigenicity with that in nude mice. To determine the sensitivity for the detection of tumor cells contamination in non-tumorigenic human somatic cells, we mixed various dose of HeLa cells in human mesenchymal stem cells and conducted tumorigenicity tests using NOG mice and Matrigel. We also performed soft agar colony formation assay, which is commonly used to detect anchorage-independent cell growth *in vitro*, and compared tumor cell detection level by soft agar with the *in vivo* tumorigenicity test.

2. Materials and methods

2.1. Cells

Human cervical cancer HeLa cells were obtained from the Health Science Research Resources Bank (HSRRB, Osaka, Japan). The cells were maintained in Eagle's minimum essential medium (Sigma), supplemented with 10% fetal bovine serum (FBS; Sigma), 0.1 mM non-essential amino acids (Life Technologies), 50 U/ml penicillin, and 50 μg/ml streptomycin (Life Technologies). Human mesenchymal stem cells (hMSCs) were purchased from Lonza and cultured in MSCGM™ medium (Lonza). Cells were cultured in a humidified atmosphere of 5% CO_2 and 95% air at 37 °C, and were passaged upon reaching 80% confluence. hMSCs were used at passage 6 and passages 6–8 for *in vivo* tumorigenicity tests and soft agar colony formation assay, respectively.

2.2. Preparation of cell suspensions for transplantation

Upon reaching approximately 80% confluence, cells were washed twice with phosphate buffered saline (PBS) and treated with 0.25% trypsin-EDTA solution (Life Technologies) for detachment from culture dishes. HeLa cells and/or hMSCs were counted and prepared in 100 μl of ice-cold HeLa cell culture medium or a 1:1 (v/v) mixture of HeLa cell culture medium and Matrigel (product #354234, BD Biosciences, San Jose, CA) for transplantation.

2.3. Tumorigenicity test with immunodeficient mice

Male BALB/cA nu/nu mice (nude; CLEA Japan, Inc., Tokyo) and male NOG mice maintained in the Central Institute for Experimental Animals (CIEA, Kanagawa, Japan) were used for *in vivo* tumorigenicity studies. Prepared cell suspensions were injected using 1 ml syringes with a 25 G needle (Terumo) into 8-week-old mice (n = 6 or 10). The mice were palpated weekly for 16 weeks to observe nodule formation at the injection site. Tumor size was assessed by external measurement of the length and width of the tumors in two dimensions using a caliper as soon as tumors reached measurable size. The tumor volume (TV) was calculated using the formula volume = 1/2 × length (mm) × (width [mm])^2. The successive engraftment was determined according to progressive nodule growth at the injection site. Mice were euthanized and necropsied when tumors reached approximately 20 mm in any dimension or when a sign of deconditioning was noted. The tumorigenicity of HeLa cells was evaluated by measuring tumor-forming capacity, which indicates the tumorigenic phenotype [8,9]. Tumor-forming capacity is defined as 50% tumor-producing dose (TPD_{50}), which represents the threshold dose of cells forming tumors in 50% of the animals. TPD_{50} values were calculated using the Spearman-Kärber method [10–12] at each time point. Not all animals transplanted with the highest dose formed tumors, in which case it was assumed that the tumor incidence of animals at 10 or 100 times the uppermost dose step (a dummy set of data) would have been 100% for the Spearman-Kärber method to be applicable [12].

The protocol of the present study was reviewed beforehand and approved by the Animal Ethics Committees of CIEA (Permit Number: 13041A) and the National Institute of Health Sciences (NIHS, Tokyo) (Permit Number: 359, 359-1, 359-2, 359-3). All animal experiments were performed according to the Ethical Guidelines for Animal Experimentation from the CIEA and the NIHS. All animals were sacrificed under isoflurane inhalation anaesthesia, and all efforts were made to minimize suffering.

2.4. Histology and immunohistochemistry

The engrafted tumors were isolated and fixed with 10% neutral buffered formalin (Wako). The paraffin-embedded sections were investigated by hematoxylin and eosin (H&E) stain and immunohistochemical studies using Bond-max stainers (Leica Biosystems). Some sections were incubated at 100 °C for 10 min in a target retrieval solution consisting of 10 mM citrate buffer (ER1; Leica Microsystems), and then placed at room temperature for 20 min. Mouse anti-human HLA class I-A, B, C monoclonal antibody (EMR8-5; Hokudo, Sapporo, Japan), and rabbit anti-vimentin monoclonal antibody (SP20; Nichirei Bioscience, Tokyo) were used as the primary antibodies. The antibodies for mouse immunoglobulin were visualized using Bond polymer refine detection kits (Leica Microsystems). Sections were counterstained with hematoxylin.

2.5. Soft agar colony formation assay

A soft agar colony formation assay was performed using a CytoSelect™ 96-well Cell Transformation Assay kit (CellBio labs, San Diego, CA) as previously described [13]. Prewarmed 25 μl of 2 × DMEM/20% FBS and 25 μl of 1.2% agar solution were mixed and

transferred onto a well of 96-well plates, and then incubated at 4 °C for 30 min to allow the bottom agar layer to solidify. HeLa cells and hMSCs were dissociated into a single cell suspension by treatment with 0.25% trypsin-EDTA solution (Life Technologies) and passed through 40 μm nylon cell strainers (BD Falcon). Next, 25 μl of cell suspensions containing serially diluted HeLa cells (0, 10, 20, 30, 50, and 100 cells) and hMSCs (1.0×10^4 cells) in DMEM/10% FBS, were mixed with 25 μl of 2 × DMEM/20% FBS and 25 μl of 1.2% agar. After being placed on the bottom agar layer, the top agar layers were immediately solidified at 4 °C for 10 min to avoid false-positive signals derived from sedimentation-induced contact between the cells. The plates were incubated with 100 μl of DMEM/10% FBS per well for 10 and 20 days at 37 °C and 5% CO_2. The medium was changed every 2–3 days. Colonies were lysed and quantified with CyQuant GR dye using a fluorometer equipped with a 485/520 nm filter set (Wallac 1420 ARVOsx multilabel counter, PerkinElmer, Boston, MA). Results were evaluated as a relative fold change of the value of negative control (hMSCs only). The lower limit of detection (LLOD) of the assay signal was calculated as the mean plus 3.3 fold the standard deviation of the measurement of the three lots of hMSCs [14].

3. Results

3.1. The tumorigenic potential of HeLa cells in nude and NOG mice

We first tried to evaluate the tumorigenic potential of human tumorigenic cells in NOG mice in the absence or presence of Matrigel, compared with that in nude mice. Namely, we examined the tumor formation of HeLa cells transplanted into the subcutaneous spaces of mice, and tumorigenic incidence was compared between nude and NOG mice for 16 weeks (Fig. 1a–c and Table 1). The development of spontaneous tumors was not observed in non-transplant mice of either strain during the period of monitoring. Nude mice, which are traditional standards for tumorigenicity testing, showed no tumor formation when HeLa cells were transplanted at a dose of up to 1.0×10^5 cells. On the other hand, NOG mice developed tumors with a lower cell transplantation dosage (1.0×10^4 cells). Transplanting HeLa cells with Matrigel considerably increased the tumor formation potential of HeLa cells in NOG mice. Notably, subcutaneous transplantation of 1.0×10^3 HeLa cells gave rise to tumors in NOG mice when embedded with Matrigel (10/10 animals) but not without Matrigel (0/10 animals). Furthermore, 60% (6/10 animals) of NOG mice formed tumors within 16 weeks when 1.0×10^2 HeLa cells were transplanted with Matrigel subcutaneously. Next, to compare tumor forming potential of nude mice and NOG mice more quantitatively, we calculated a 50% tumor producing dose, TPD_{50}, of HeLa cells in NOG and nude mice. At the end of monitoring for 16 weeks, NOG mice exhibited $TPD_{50} = 1.3 \times 10^4$ when injected with HeLa cells in the absence of Matrigel (Table 1). As expected, tumorigenic potential of HeLa cells was enhanced 30-fold when transplanted in NOG mice compared with that in nude mice ($TPD_{50} = 4.0 \times 10^5$ at week 16). Furthermore, tumorigenic potential of HeLa cell was enhanced 5000-fold when HeLa cells are embedded with Matrigel and transplanted in NOG mice ($TPD_{50} = 7.9 \times 10$ at week 16) compared with that in nude mice without Matrigel. Thus, NOG mice showed superior tumor forming potential when the tumor cells are embedded with Matrigel.

Transplanted cells progressively formed a large spheroid tumor at the inoculation site without invading host subcutaneous tissue (Fig. 2d). Tumor mass increases in a dose- and time-dependent manner in both mouse strains (Fig. 2a–c). To confirm the origin of tumors engrafted in the NOG mice, embedded tissue sections were stained with anti-human HLA antibody. The immunohistochemical analysis demonstrated that the engrafted tumors originated from human cells (Fig. 2e). No histological difference was observed between tumor in nude mice and that in NOG mice (data not shown).

3.2. Detection of tumors in NOG mice inoculated with HeLa cells spiked into hMSCs

Next we attempted to determine the characteristics of the test using NOG mice and Matrigel for detection of tumorigenic cellular impurities in human somatic cells. For this end, HeLa cells (1.0×10, 1.0×10^2, 1.0×10^3, and 1.0×10^4) were spiked into 1.0×10^6 hMSCs, and then subcutaneously transplanted into NOG mice with Matrigel. Tumor formation at the transplanted site was continuously monitored for 16 weeks. Subcutaneous transplantation of hMSCs alone in NOG mice did not generate tumor in any mice during the monitoring period (Table 2). Within 16 weeks after transplanation, 50% of the NOG mice (3/6 animals) generated subcutaneous tumors derived from 1.0×10^2 HeLa cells spiked in 1.0×10^6 hMSCs (Fig. 3a). The TPD_{50} of HeLa cells transplanted in NOG mice with 1.0×10^6 hMSCs and Matrigel was 1.0×10^2 at week 16, which was almost the same as the TPD_{50} transplanted with HeLa cells alone (Tables 1 and 2). These results indicated that *in vivo* tumorigenicity tests using NOG mice and Matrigel are able to detect over 0.01% HeLa cell contamination in hMSCs, which is equivalent to a single tumor cell contamination in 10,000 somatic cells. To determine sensitivity of tumorigenicity tests using NOG mice, we spiked 1.0×10 (0.0001%) and 1.0×10^2 (0.001%) HeLa cells into hMSCs (1.0×10^7 cells), which was tenfold the dose used in the previous experiments, and subcutaneously transplanted them into NOG mice with Matrigel. Two and out of 6 NOG mice inoculated with 1×10^2 HeLa cells generated subcutaneous tumors within 16 weeks when a higher dose of hMSCs was co-transplanted (Fig. 3b). It is of note that one out of 6 mice transplanted with 1×10 HeLa cells and 1×10^7 hMSCs also showed tumor formation. The TPD_{50} of HeLa cells transplanted with 1.0×10^7 hMSCs and Matrigel in NOG mice was 1.8×10^2 at week 16 (Table 2). These results are quite

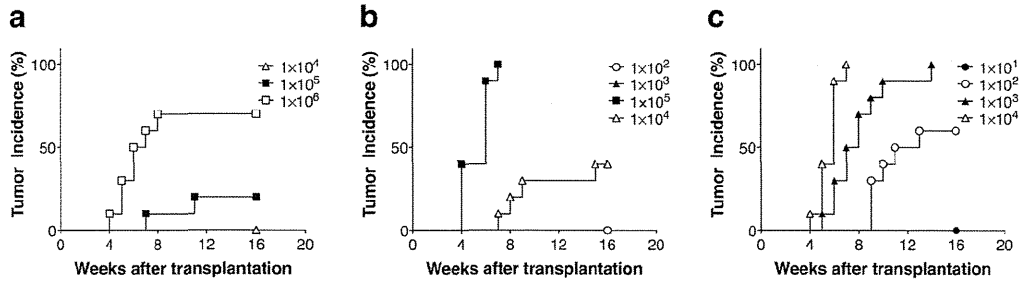

Fig. 1. Tumor incidence of HeLa cells in nude and NOG mice. The tumor formation of HeLa cells transplanted into the subcutaneous spaces of mice was examined for 16 weeks. The relationships between the dose and the tumorigenic incidence of HeLa cells in nude mice (a) and NOG without (b) or with (c) Matrigel are presented (n = 10 in each group).

Table 1
Tumor-forming capacity of HeLa cells in nude and NOG mice.

Strain	Group	Tumor incidence at indicated HeLa cell dose at 16w								TPD_{50} at week 16	Fold-change in TPD_{50} (vs. nude mice)
		0	1×10	1×10^2	1×10^3	1×10^4	1×10^5	1×10^6	1×10^7		
Nude	HeLa	0/10[a]	–	–	–	0/10	2/10	7/10	(10/10)[b]	4.0×10^5	1.0
NOG	HeLa	0/10	–	0/10	0/10	4/10	10/10	–	–	1.3×10^4	3.0×10
NOG	HeLa w/MG	0/10	0/10	6/10	10/10	10/10	–	–	–	7.9×10	5.0×10^3

–: Not tested.
MG: Matrigel.
[a] No. of mice in which tumors formed/total no. of mice inoculated.
[b] Since not all animals inoculated with the highest dose (10^6) formed tumors, it was assumed that the tumor incidence of animals at an even higher dose step (a dummy set of data) would have been 100% for the Spearman-Kärber method to be applicable.

consistent with those without a mixture of hMSCs (Fig. 1c), demonstrating that HeLa cells can grow under subcutaneous environments of NOG mice without significant effect from co-tansplanted hMSCs. Taken together, our results indicated that *in vivo* tumorigenicity tests with NOG mice in the combination with Matrigel has the ability to detect 100 HeLa cells spiked into hMSCs in almost half of mice.

Morphological observation of tumors originated from HeLa cells spiked in hMSCs and HeLa cells alone was identical (Figs. 2d and 3c). The immunohistochemical analysis of the tissue sections using anti-human HLA monoclonal antibody clearly demonstrated that the engrafted tumors originated from human cells (Fig. 3d). Vimentin, an intermediated filament protein, is known to express in the process of epithelial to mesenchymal transition and is commonly used as one of the markers of mesenchymal stem cells [15,16]. Negative staining with anti-vimentin antibody suggested that formed tumors were attributed to the exceeding growth of HeLa cells (Fig. 3e).

3.3. Changes of TPD_{50} values depending on the time course

The tumor development of HeLa cells in nude and NOG mice under various conditions are shown as the transition of TPD_{50} at weekly intervals. Nude and NOG mice inoculated with HeLa cells without Matrigel demonstrated only a slight decrease in TPD_{50} values from 8 weeks following injection (Fig. 4). On the other hand, TPD_{50} values rapidly decreased until 12 weeks and then almost reached a plateau until 16 weeks when NOG mice were inoculated with cells in combination with Matrigel. These results suggest that Matrigel is able to support the growth of transplanted small number of tumor cells that cannot survive without Matrigel, and a tumor originated from small number of tumorigenic cells takes time to form visible mass.

3.4. Soft agar colony formation assay for detection of HeLa cell contamination

The soft agar colony formation assay is a suitable method to monitor anchorage-independent cell growth and a well-known *in vitro* assay for the detection of malignant transformed cells [17,18]. HeLa cells enclosed by soft agar showed progressive formation of colonies (Fig. 5a), whereas hMSCs did not form any colonies in a soft agar media with 1×10^4 cells/well by day 20 (Fig. 5b and c). We next spiked several concentrations of HeLa cells into 1×10^4 hMSCs to determine the minimum number of HeLa cells required for growth in a soft agar media. More than 0.2% spiked

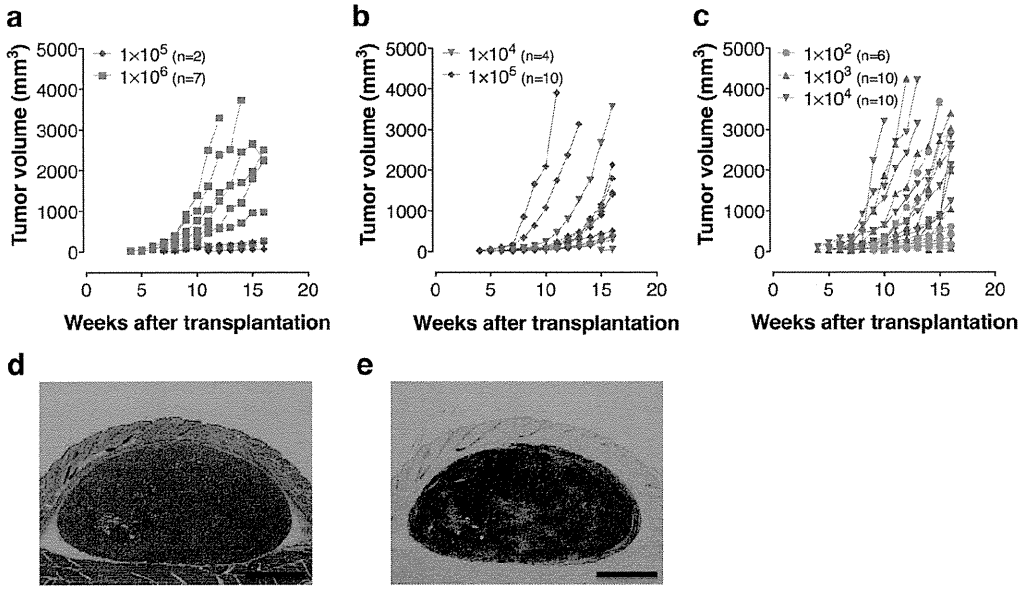

Fig. 2. Characterization of subcutaneous tumors formed by transplantation with HeLa cells in nude and NOG mice. Growth curves of subcutaneous tumors formed by inoculation with various dosages of HeLa cells were presented in respective mice (a: nude; b: NOG w/o Matrigel; c: NOG w/Matrigel). The tumor volume (TV) was calculated using the formula volume = 1/2 × length (mm) × (width [mm])^2. The successive engraftment was determined according to progressive nodule growth at the injection site. Mice were euthanized and necropsied when tumors reached approximately 20 mm in any dimension or when a sign of deconditioning was noted. Representative images from histology and immunohistochemistry analyses of subcutaneous tumors in NOG mice formed by transplantation with 1.0×10^2 HeLa cells suspended in Matrigel (d and e). Serial sections were stained with H&E (d) and HLA antibody (e) (magnification, 40×; scale bars, 1 mm).